NASA Contractor Report 3479

Analysis of Rotary Balance Data for the F-15 Airplane Including the Effect of Conformal Fuel Tanks

Billy Barnhart

CONTRACT NAS1-16205
APRIL 1982

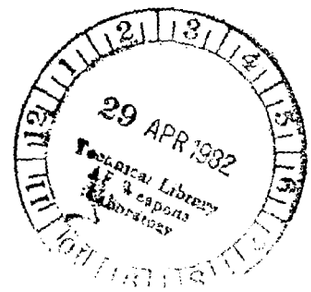

NASA Contractor Report 3479

Analysis of Rotary Balance Data for the F-15 Airplane Including the Effect of Conformal Fuel Tanks

Billy Barnhart
Bihrle Applied Research, Inc.
Jericho, New York

Prepared for
Langley Research Center
under Contract NAS1-16205

National Aeronautics
and Space Administration

Scientific and Technical
Information Branch

1982

SUMMARY

F-15 rotary balance data have been analyzed, and the influence of control deflections, Reynolds number and airplane components, i.e., body, wing, horizontal and vertical tails, as well as conformal tanks, on the aerodynamics up to 90° angle of attack are discussed. Steady-state spin mode predictions using these data are presented, which show excellent correlation with spin tunnel and flight-test results.

Generally, the data show damped yawing-moment slopes with rotation at all angles of attack, and good control effectiveness. Differences in the rotary aerodynamics due to the addition of conformal tanks are minimal. The small differences in the region of the flat spin do, however, indicate that the resulting spin mode would be slightly flatter and faster for a conformal tank equipped airplane. The addition of conformal tanks also may make the airplane more departure susceptible.

INTRODUCTION

The NASA Langley Research Center is conducting an investigation to determine the influence of the addition of conformal fuel tanks on the spin and recovery characteristics of the Air Force/McDonnell Douglas F-15 airplane. As part of this effort, rotary balance data were measured for a 1/12-scale F-15 model, both with and without conformal fuel tanks, to provide a data base for the analysis of free-spinning model tests conducted at the Langley Spin Tunnel. Photographs of the 1/12-scale model installed on the rotary balance located in the Langley Spin Tunnel are shown in figure 1, and a three-view drawing of the basic model is presented in figure 2. The conformal fuel tanks are installed on the outboard side of each engine nacelle, as shown in figure 3.

A rotary balance is used to measure the forces and moments acting on an airplane model while it is subjected

to steady rotational flow conditions. The model is mounted on an internal strain gauge balance, which is attached to the rotary balance apparatus. During testing, the forces and moments are measured while the model is rotated about a vertical axis at the center of the tunnel.

Reference 1 contains the six-component rotary balance data measured for the basic airplane, presented without analysis, as well as a detailed description of the test equipment, the model, and the test procedures. The same information is presented in reference 2 for the conformal tank configuration. An analysis of these data is presented herein, including the effect of control deflections, airplane components, and the influence of conformal fuel tanks. Additionally, comparison of the static aerodynamics measured during the rotary balance tests (at $\Omega b/2V=0$) with other static F-15 data, and a discussion of the Reynolds number effects are included. Steady-state spin modes are also predicted from the rotary balance data for the airplane, both with and without conformal tanks, and the results are compared to preliminary spin tunnel and flight-test results.

SYMBOLS

The units for physical quantities used herein are presented in the International System of Units and U.S. Customary Units. The measurements were made in the U.S. Customary Units; equivalent dimensions were determined by using the conversion factors given in reference 3.

b	wing span, m (ft)
$\bar{c}$	mean aerodynamic chord, m (ft)
C_ℓ	rolling-moment coefficient, $\frac{\text{Rolling moment}}{qSb}$
C_m	pitching-moment coefficient, $\frac{\text{Pitching moment}}{qS\bar{c}}$
C_n	yawing-moment coefficient, $\frac{\text{Yawing moment}}{qSb}$
q	free-stream dynamic pressure, N/m^2 (lb/ft^2)
R_e	Reynolds number

S	wing area, m^2 (ft^2)
V	free-stream velocity, m/sec (ft/sec)
α	angle of attack, deg
β	angle of sideslip, deg
Ω	angular velocity about spin axis, rad/sec
$\frac{\Omega b}{2V}$	spin coefficient, positive for clockwise spin
δ_a	aileron deflection, positive when right aileron is down, $(\delta_{a_{right}} - \delta_{a_{left}})/2$, deg
δ_d	differential horizontal tail deflection, positive when right panel is down, $(\delta_{d_{right}} - \delta_{d_{left}})/2$, deg
δ_e	symmetrical horizontal tail deflection, positive when trailing edge is down, deg
δ_r	rudder deflection, positive when trailing edge is to left, deg

Abbreviations:

CFT	conformal fuel tanks
cg	center of gravity
SR	spin radius

PRESENTATION OF RESULTS

Selected rotary balance data are presented herein for analysis purposes. These data are presented as plots of body axis aerodynamic coefficients as functions of the nondimensionalized rotation rate, $\Omega b/2V$, at constant angles of attack. The spin axis for the presented data passed through the airplane cg for angles of attack above 30^o, and at a full-scale distance of 1.8m (72 in.) forward of the cg location for angles of attack of 30^o or less. The data were measured at a Reynolds number of approximately 211,000 based on wing chord, and about a cg location of $0.26\bar{c}$.

The rolling and yawing-moment coefficients are damped for data lying in the second and fourth quadrants and propelling for data in the first and third quadrants, when plotted as functions of $\pm\Omega b/2V$.

DISCUSSION

Effect of Body, Wing, and Tails

The model was constructed such that the various components were removable for component build-up testing. In this manner, the influence of each component on the aerodynamic data could be determined by first testing the body alone and then adding each of the other components one by one. For these tests, data were measured for the body alone, body-wing, body-wing-vertical tail, and body-wing-horizontal tail combinations, as well as for the complete airplane. This was done for the basic F-15 body (which included the engine nacelles), and for the body with conformal fuel tanks.

Component build-up plots of each of the three aerodynamic moments are presented in figures 4 through 6 for the conformal fuel tank configuration. These figures show the data for the body alone and for the successive addition of each component.

Pitch Characteristics:

Component build-up plots of the pitching-moment coefficient vs $\frac{\Omega b}{2V}$ are shown in figure 4 for selected angles of attack. Examination of these plots shows that the body alone generates a nose-up pitching moment at all angles of attack. The wing introduces a nose-down increment. The addition of the horizontal tail adds a further nose-down increment sufficient to make the airplane have a nose-down C_m. Further, the static C_m vs angle-of-attack curve is stable, i.e., the pitching moment becomes more nose-down with increasing angle of attack. The effect of rotation rate is to further increase the magnitude of the nose-down moment.

The C_m curves are generally fairly symmetrical for clockwise and counter clockwise rotations, except at angles of attack near 60°, as seen in figure 4d. At these angles of attack, the curves show an unsymmetrical characteristic starting with the body alone that is similar to C_m curves at nonzero sideslip angle. This is evidently due to unsymmetrical vortex shedding from the nose at these angles of attack; evidence of which also appears in the other aerodynamic moment coefficients.

Roll Characteristics:

Figure 5 presents component build-up plots of the rolling-moment coefficient vs $\frac{\Omega b}{2V}$ for selected angles of attack. It is seen that the body is slightly propelling up to approximately 40° angle of attack, and is then fairly neutral for higher angles of attack. As would be expected, the wing contributes, by far, the bulk of the rolling-moment coefficient of the total airplane for angles of attack less than 40°, with the horizontal and vertical tails supplying only relatively small variations from the body-wing curves.

At 20° angle of attack, figure 5a, the wing provides damping at all $\Omega b/2V$'s. However, the wing is propelling for $\Omega b/2V$ magnitudes less than approximately 0.35 at 30° angle of attack (figure 5b). Propelling rolling moments caused by the wing in the stall and post-stall angle-of-attack region are not unusual.

In figure 5c, it is seen that at 40° angle of attack the horizontal tail is providing a significant propelling moment increment, such that the total airplane exhibits a propelling C_ℓ moment. For angles of attack greater than 40°, figures 5d and 5e, the horizontal tail supplies a substantial propelling C_ℓ increment only at the higher $\Omega b/2V$'s. This may be characteristic of airplanes with wide afterbodies; however, for most other configurations, the horizontal tail does not contribute any significant rolling moment at any angle of attack when compared to the wing contribution.

It is normal for the airplane to lose all damping of the body axis rolling moment at 80° to 90° angle of attack. This is not significant, however, because the yawing moment is the dominant driving moment about the velocity vector at these angles of attack and thus determines whether a flat spin shall occur. If a flat spin does exist, the airplane will assume a small sideslip angle sufficient to balance out any rolling moment due to rotation.

Yaw Characteristics:

The component build-up plots for the yawing-moment coefficient vs $\Omega b/2V$ are presented in figure 6. Up to 20° angle of attack, the body and body-wing combinations provide very little C_n; virtually all the yawing moment is supplied by the vertical tails (figure 6a). At 30° angle of attack, however, even though the bulk of the damping is being provided by the vertical tails, the body and the wing are providing a small amount of damping (figure 6b). By 40° angle of attack, figure 6c, the body-wing combination is supplying most of the damping for $\Omega b/2V$ values between ± 0.2, with the vertical tails supplying a large percentage of the damping only for higher rotation rates. As is the case for most airplanes, through this angle-of-attack range the addition of the wing produces a beneficial interference effect on the body, resulting in increased damping.

In the angle-of-attack range from approximately 50° to 70°, the body exhibits a yawing-moment offset, the magnitude of which is greatest near 60° (figure 6d). This moment is evidently due to unsymmetric vortex shedding at the aircraft nose, mentioned previously. This phenomenon is a characteristic of high fineness-ratio noses. Although the magnitude of the offset at zero rotation rate at full-scale Reynolds number may be less than that measured at low Reynolds number, the trend of the data will be the same, i.e., if the low R_e

data show a damped (negative) or propelling slope through zero rotation, the full-scale data would also exhibit the same characteristic.

The C_n characteristics of the body predominate over most of the $\Omega b/2V$ range at 60° angle of attack. Here, also, it is seen that the addition of the vertical tails provides a damping increment which is, however, more than cancelled by the further addition of the horizontal tails. This is characteristic of most airplanes at high angles of attack.

At 80° angle of attack, figure 6e, the C_n offset is gone and the body alone curve is damped. The addition of the wing results in less damping at the lower $\Omega b/2V$'s and more at the higher values. Without the presence of the horizontal tail, the vertical tails provide damping; however, with the horizontal tail the vertical tail effect is negated for rotation rates less than approximately 0.3.

Effect of Conformal Tanks:

Component Data:

The effect of conformal tanks on the body alone pitching and rolling characteristics is minimal. Figures 7a and b present plots of C_n vs $\frac{\Omega b}{2V}$ for 40° and 80° angle of attack, respectively. It is seen that the addition of conformal tanks to the body alone results in decreased damping moment through this angle-of-attack range.

The addition of the CFT's to the body-wing combination had negligible effect on the rolling-moment coefficient, as it did on the body alone, except near 40° angle of attack. At this angle of attack, the addition of the CFT's generally contributes a propelling increment to the basic body-wing configuration (figure 8). This is the largest difference that was seen in any aerodynamic coefficient as the result of adding conformal tanks. The yawing-moment coefficients for the body-wing combination show little difference due to addition of the

CFT's, other than what was observed for the body alone, and the pitching moment was negligibly affected.

The addition of the vertical or the horizontal tails does not significantly alter the influence of the conformal tanks on the aerodynamic data beyond that observed for the body alone and body-wing combination except to slightly ameliorate the differences noted.

Total Airplane Data:

The conformal fuel tanks have no significant influence on the pitching-moment characteristics of the total airplane. For the rolling-moment coefficient, the data with and without conformal fuel tanks are virtually identical throughout the angle-of-attack range, except at 40° angle of attack (figure 9) where it is seen that the CFT configuration is significantly more propelling in roll than the basic configuration. This is the same characteristic that was first seen for the body-wing combination. Consequently, it would be anticipated that the airplane with conformal tanks would possibly be more departure susceptible due to the propelling rolling moment in the 40° angle-of-attack range.

The effect of the conformal tanks on the yawing-moment coefficient is minimal for angles of attack through 70°. At 80° angle of attack (figure 10), it is seen that the conformal fuel tank equipped model exhibits less damping C_n for $\frac{\Omega b}{2V}$ values near zero.

Pro-Spin Control Data:

Figure 11 presents plots of yawing-moment coefficient vs $\frac{\Omega b}{2V}$ at constant angles of attack for both the basic F-15 and the CFT equipped airplane with pro-spin controls for clockwise ($+\frac{\Omega b}{2V}$) spins. For angles of attack through 60°, there is no significant difference between the two airplanes. At 50° and 60° angle of attack, the airplanes exhibit propelling C_n's

with pro-spin controls for a large range of clockwise $\frac{\Omega b}{2V}$'s. This is due to both the pro-spin controls and the large positive yawing-moment offset resulting from the asymmetric vortex shedding at the nose. At the higher angles of attack (figure 11c), it is seen that the conformal tank configuration crosses the zero C_n axis at a greater $\frac{\Omega b}{2V}$ value than the basic airplane. This would indicate the possibility that the CFT airplane could have a faster and, thus, possibly flatter spin with pro-spin controls than the basic airplane.

Recovery Control Data:

At 80° angle of attack, figure 12a, substantial recovery yawing moment is observed for both the basic and CFT equipped airplanes with controls set for recovery from a clockwise ($+\frac{\Omega b}{2V}$) spin. There is slightly more recovery moment for the basic configuration in the $\frac{\Omega b}{2V}$ range of 0.2 to 0.3, which is the probable flat spin rotation rate. By 70° angle of attack, figure 12b, there is no significant difference between the two configurations. Figure 12c shows the yawing-moment coefficient at 60° angle of attack. Here it is seen that there is little recovery moment for either configuration at this angle of attack; there is actually some pro-spin moment for low $\frac{\Omega b}{2V}$ values. It could be anticipated that either airplane configuration would be slowed in its recovery through this angle-of-attack range. As mentioned previously, the magnitude of the C_n offset could be Reynolds number dependent, such that less propelling moments may exist at full-scale Reynolds number. At the lower angles of attack, figure 12d, there is negligible difference between the two airplanes.

Effect of Controls

Figure 13 presents yawing-moment coefficient plots at selected angles of attack for all neutral controls and for a pro-spin and a recovery control setting when referenced to a clockwise spin. The pro-spin control setting consisted of

6° of differential tail and 20° aileron, each set against the spin, and a 15° rudder deflection set with the spin. The recovery control setting was 11° differential tail, and 20° aileron set with the spin, and 30° rudder set against the spin. All of the plots are for the F-15 model with conformal fuel tanks. Data for the same control settings for the airplane without conformal tanks are presented in reference 1. The effect of control settings is similar for both configurations.

The yawing-moment coefficient data for 30° angle of attack are generally characteristic of the low angle-of-attack C_n data (figure 13a). The effect of controls appears to be fairly constant over the $\frac{\Omega b}{2V}$ range, and the incremental yawing-moment coefficient between the neutral and pro-spin and between the neutral and recovery control settings is roughly proportioned to the differential tail deflection. In the angle-of-attack range of 50° to 70° (figures 13b and c), much of the linearity has disappeared, most probably due to the interaction of the asymmetric vortex shedding. At 60°, some propelling moment is still present even with recovery controls, due to the large C_n offset. By 80° angle of attack, figure 13d, the incremental effect of control deflection on yawing-moment coefficient is more nearly linear than it was in the 50° to 70° angle-of-attack range, and a large recovery moment is observed for recovery controls.

Effect of Differential Tail Deflection

The effect of differential tail deflection alone is shown in figures 14 and 15 for the rolling and yawing-moment coefficients, respectively. For angles of attack up to 30° (figures 14a and b), the incremental rolling-moment coefficient due to differential tail deflection is reasonably linear and constant with rotation. For angles of attack greater than 30°, however, the control effectiveness is generally no longer

linear with deflection nor constant with rotation (figures 14c and d). At the higher angles of attack, there is generally a small incremental rolling moment due to a 6^{o} differential tail deflection, but no additional increment is realized by increasing the deflection (figure 14e).

The yawing-moment coefficient plots show that at 20^{o} angle of attack there is only a small proverse increment due to differential tail deflection (figure 15a). By 30^{o} angle of attack and above, the effect of differential tail deflection is always to produce adverse yaw. At the higher angles of attack, the incremental yawing moments due to differential tail deflection are significant, but are not generally linear with control deflection nor constant with rotation rate. The above results indicate that in the high angle-of-attack flight regime the differential tail is an effective yaw producer rather than a roll controller.

Predicted Spin Modes

Prediction of equilibrium steady-state spin modes can be quickly made using rotary balance aerodynamic data. A computer search is used to determine what, if any, conditions (i.e., angle of attack, rotation rate, etc.) result in a balance of the three aerodynamic and inertial moments. An outline of the method and a historical background are contained in reference 4.

The predictions of clockwise spins for the F-15 airplane with and without conformal fuel tanks are contained in Table I. For pro-spin controls, consisting of ailerons and differential tails set against the spin, and rudder deflected with the spin, the results show that the CFT configured airplane exhibits a very slightly flatter and faster flat spin mode compared to the basic airplane.

Table I also shows the predicted spin modes for each configuration with lateral-directional controls neutralized and stick full aft. For this control setting, moderately flat spin

modes at 65° and 66° are predicted for the basic and the CFT configuration, respectively.

With recovery controls, the flat spin mode is eliminated and both configurations show a weak equilibrium at 58° angle of attack. This equilibrium is due to the large positive yawing-moment offset in this angle-of-attack region, and for this model, therefore, would only occur for clockwise rotations.

Free-spinning tests performed in the Langley Spin Tunnel showed excellent correlation with the predicted spin modes for pro-spin controls, as demonstrated in Table II. The preliminary spin tunnel results showed that the CFT configured model did spin slightly flatter and faster than the basic model, as predicted.

Flight-test results also agreed closely with predictions. A typical flight-test spin time history, from reference 6, showed that the full-scale airplane exhibited a 75° right spin at approximately 3 seconds per turn. The correlation between the predicted steady spin mode and that observed during flight test is considered excellent, especially when it is appreciated that flight test cannot often achieve the idealized situation available to the analyst. The spin time history in reference 6, for example, showed that the pro-spin controls were removed at approximately the time the quoted peak rotation rate was obtained so that it is uncertain whether the airplane had achieved its final steady-state spin at that time.

The static pitching-moment coefficient for this airplane shows a noticeable shift due to Reynolds number, as discussed in the next section. The influence of this R_e effect on the predicted spin modes was investigated by adding a nose-down incremental pitching-moment coefficient sufficient to make the static rotary balance C_m agree with those measured during Ames high Reynolds number tests. This resulted in only a slight change in the predicted flat spin mode, with the angle of

attack going from 80^{o} to 77^{o} while the rate of rotation was unchanged.

With the lateral controls undeflected and the stick full aft, the free-spinning basic F-15 model showed an oscillatory spin at 4.8 seconds per turn with the angle of attack varying between 55^{o} and 67^{o} (reference 5). The rotary balance predicts a spin mode at 65^{o} and 5.1 seconds per turn for the stick aft (Table I). Predicted spin equilibrium points may not result in steady spins; the spin prediction technique assumes that the angular accelerations are zero. If the accelerations are, in fact, near zero, a steady spin will occur. If, however, the stability of the spin mode is weak, such that the accelerations do not approach zero, an oscillatory spin may result in the angle-of-attack region of the predicted equilibrium, as is apparently true in this case.

With recovery controls, the spin-tunnel results showed recoveries occurring for the basic airplane in approximately four turns (reference 5), and in approximately six turns for the conformal tank equipped model. Flight-test results for the basic F-15 also showed that the basic airplane recovered in approximately four turns.

In none of the experimental tests did the airplanes seek the predicted weak equilibrium at 58^{o} angle of attack. However, it was noted from the flight-test time histories that the angle of attack remained near 60^{o} for some time before continuing to decrease, while the rotation rate decreased more slowly. The flight-test results further indicate that "the aerodynamic recovery capability in the right spin was significantly decreased at 62^{o} to 65^{o} AOA. In the left spin, decreased capability was not exhibited at these AOA's." These results indicate that a yawing-moment offset, observed during the rotary balance tests at these angles of attack, was also present on the full-scale airplane. In this case, the yawing moments were offset positively for both the rotary balance model and the airplane, though this need not necessarily be true.

Effect of Reynolds Number

The ability to predict airplane spin characteristics has been greatly amplified by the existence of viable rotary balance data. The data measured by the rotary balance in the Langley Spin Tunnel are measured at low Reynolds number. Since there is, currently, no operational facility which can provide comparable data at the high R_e approaching that of the full-scale airplane, it is not possible to measure the Reynolds number effects on the rotary data. To provide some measure of the effect of R_e, however, the static rotary data (measured at $\Omega b/2V=0$) can be compared to static force test results gathered at higher R_e. Approximate values of C_{ℓ_β} and C_{n_β} were calculated as $\Delta C_\ell/\Delta\beta$ and $\Delta C_n/\Delta\beta$ using $\pm 10^\circ$ sideslip data at zero $\Omega b/2V$. These data are shown in figures 16 and 17 for both the basic F-15 and the airplane with conformal tanks.

The static rotary balance data exhibit stable C_{ℓ_β}'s at all angles of attack except for a small region near stall at 30°. Also shown in figure 16 is comparable data measured for the F-15 in the Ames 12-foot pressure tunnel at a Reynolds number of 4.8×10^6, based on wing chord (from reference 7). Comparison of these data to the static rotary balance data shows that the lower R_e rotary balance data agrees well with that measured at a much higher R_e, except near 30° angle of attack. At this angle of attack, the Ames data do not show the loss of dihedral effect seen in the rotary balance data. The C_{n_β} values are stable for angles of attack less than approximately 20°, and unstable for higher angles. The Ames higher Reynolds number data agree reasonably well with the rotary balance data up to approximately 45°. For angles of attack greater than 45°, the Ames data show essentially neutral C_{n_β} values whereas the rotary balance data remain slightly unstable.

The static pitching-moment coefficient (measured at $\Omega b/2V=0$) is plotted as a function of angle of attack in figure 18. Also shown are currently unpublished high-angle-of-attack C_m data measured for an F-15 model at the Ames 12-foot pressure tunnel for two Reynolds numbers during 1981. Both the Ames data sets show generally more negative pitching-moment coefficients at a given angle of attack than was measured on the rotary balance.

The difference in static pitching-moment coefficient is due to Reynolds number effects. This is demonstrated in figure 19, which is based on data taken from reference 7, showing the variation of C_m with R_e for this airplane at three angles of attack. These results indicate that predicted spin modes based on low Reynolds number rotary balance data may differ slightly from those observed at full-scale Reynolds number, since the pitching moment is instrumental in determining the spin modes. It was seen, however, as mentioned in the previous section, that the correlation between the predicted flat spin using low Reynolds number rotary data and the flight-test result was excellent. For this airplane, at least, the low R_e rotary balance data are adequate for spin prediction.

CONCLUDING REMARKS

The rotary balance data indicate that the F-15 is basically a good aerodynamic design for spin resistance; the airplane has a yawing-moment coefficient vs $\Omega b/2V$ curve that has a damped slope at all angles of attack; it has a stable pitching moment, and the control effectiveness remains good throughout the angle-of-attack range, providing aerodynamic recovery moments at the flat spin attitude. There is, however, a nonzero yawing-moment coefficient at zero rotation and sideslip angle in the region near 60° angle of attack, which evidently slows recoveries. There is some propelling rolling-moment coefficient in the post-stall region which could indicate a departure tendency, which would be greater for the conformal tank equipped

airplane.

Generally, differences in the rotary aerodynamic data due to the addition of conformal fuel tanks are minimal. However, the small differences at the flat spin attitudes and rotation rate are sufficient to cause the CFT equipped airplane to spin slightly flatter and faster. This result was predicted from the aerodynamic data and observed during preliminary free-spinning tests. Free-spinning tests showed a significant decrease in spin recovery capability for the CFT equipped model, which is not readily apparent from the rotary data. However, this could result from the fact that the CFT airplane spins flatter and faster and thus requires more time for recovery. Also, there is a small reduction in the recovery moment available for the CFT airplane with recovery controls, although the difference appears slight.

Predicted spin modes using the rotary balance data show good agreement with flight-test and spin-tunnel results. A shift in the static pitching-moment curve due to a Reynolds number effect was demonstrated to have a minimal effect on the predicted flat spin mode. This study indicates that it is possible to adequately predict full-scale spin modes employing low R_e rotary balance data.

REFERENCES

1. Barnhart, B.: F-15 Rotary Balance Data for an Angle-of-Attack Range of 8° to 90°. NASA CR-3478, 1982.
2. Barnhart, B.: Rotary Balance Data for a Conformal Fuel Tank Equipped F-15 for an Angle-of-Attack Range of 8° to 90°. NASA CR-3516, 1982.
3. Standard for Metric Practice. E 380-79, American Society for Testing and Materials, c.1980.
4. Bihrle, W., Jr.; and Barnhart, B.: Spin Prediction Techniques. AIAA-80-1564-CP, Aug. 1980.
5. Bowman, James S., Jr.; White, William L.; and Lee, Henry A.: Spin-Tunnel Investigation of a 1/30-Scale Model of the McDonnell Douglas F-15 Airplane - COORD NO. AF-AM-010, NASA TM SX-3570, U.S. Air Force, 1977.
6. Arent, Lauren E.; Wilson, Donald B.; and Taylor, John H.: F-15A Approach-to-Stall/Stall/Post-Stall Evaluation, Final Report. U.S. Air Force, AFFTC-TR-75-32, Jan. 1976. (Available from DTIC as AD B045 115L.)
7. Massa, John D.: High Angle of Attack Tests on a 7.5 Percent Scale Model F-15 in the Ames 12-Foot Pressure Wind Tunnel. MDC A0647, Oct. 1970.

TABLE I.- PREDICTED SPIN MODES FOR CLOCKWISE SPINS

CONTROL DEFLECTIONS				BASIC F-15 PREDICTED SPIN				CFT F-15 PREDICTED SPIN				COMMENTS
δ_e deg	δ_d deg	δ_a deg	δ_r deg	α deg	$\frac{\text{sec}}{\text{turn}}$	$\frac{\Omega b}{2V}$	V m/sec (ft/sec)	α deg	$\frac{\text{sec}}{\text{turn}}$	$\frac{\Omega b}{2V}$	V m/sec (ft/sec)	
0	+6	+20	-15	80	2.7	0.21	74 (244)	81	2.3	0.23	76 (248)	Pro-spin controls
-25	0	0	0	65	5.1	0.10	83 (272)	66	5.6	0.09	80 (262)	Lateral-directional controls neutralized, stick aft
0	-6	-20	+30	58	5.4	0.09	82 (268)	58	5.9	0.08	83 (273)	Recovery controls (weak equilibrium)

TABLE II.- COMPARISON OF PREDICTED SPIN MODES WITH PRELIMINARY SPIN TUNNEL RESULTS

CONFIGURATION	CONTROLS				PREDICTED SPINS				SPIN TUNNEL RESULTS			
	δ_e deg	δ_d deg	δ_a deg	δ_r deg	α deg	$\frac{\text{sec}}{\text{turn}}$	$\frac{\Omega b}{2V}$	V m/sec (ft/sec)	α deg	$\frac{\text{sec}}{\text{turn}}$	$\frac{\Omega b}{2V}$	V m/sec (ft/sec)
Basic F-15	0	+6	+20	-15	80	2.7	0.21	74 (244)	81	2.4	0.24	71 (234)
F-15 w/CFT's	↓	↓	↓	↓	81	2.3	0.23	76 (248)	84	2.1	0.28	71 (234)
Basic F-15	0	-11	-20	+30	56	6.1	0.08	85 (278)	~4 turn recovery			
F-15 w/CFT's	↓	↓	↓	↓	56	6.5	0.07	87 (287)	~6 turn recovery			

NASA
L-81-6243

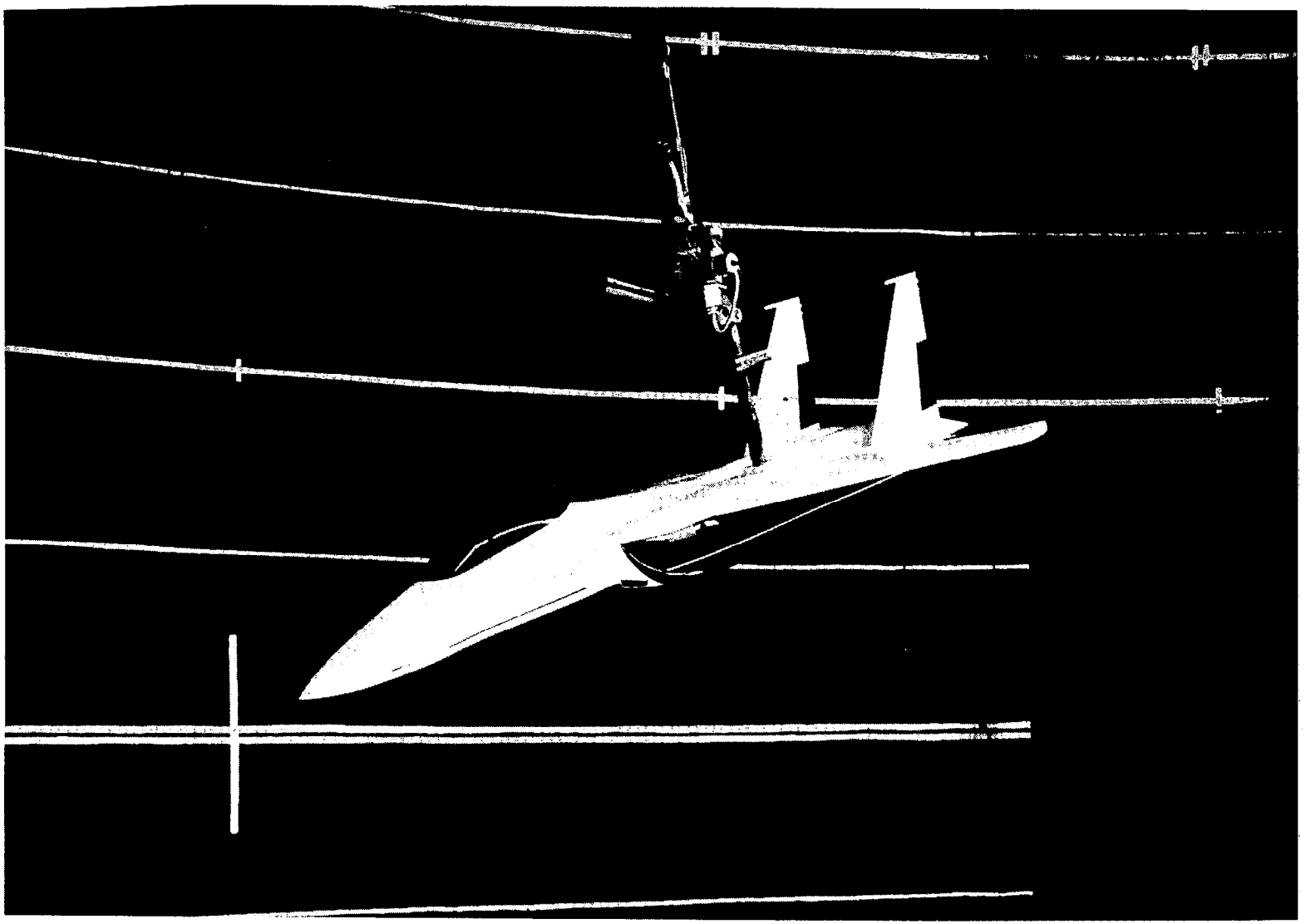

a) Front quarter view

Figure 1.- Photograph of 1/12-scale model installed on the rotary balance apparatus.

NASA
L-81-6247

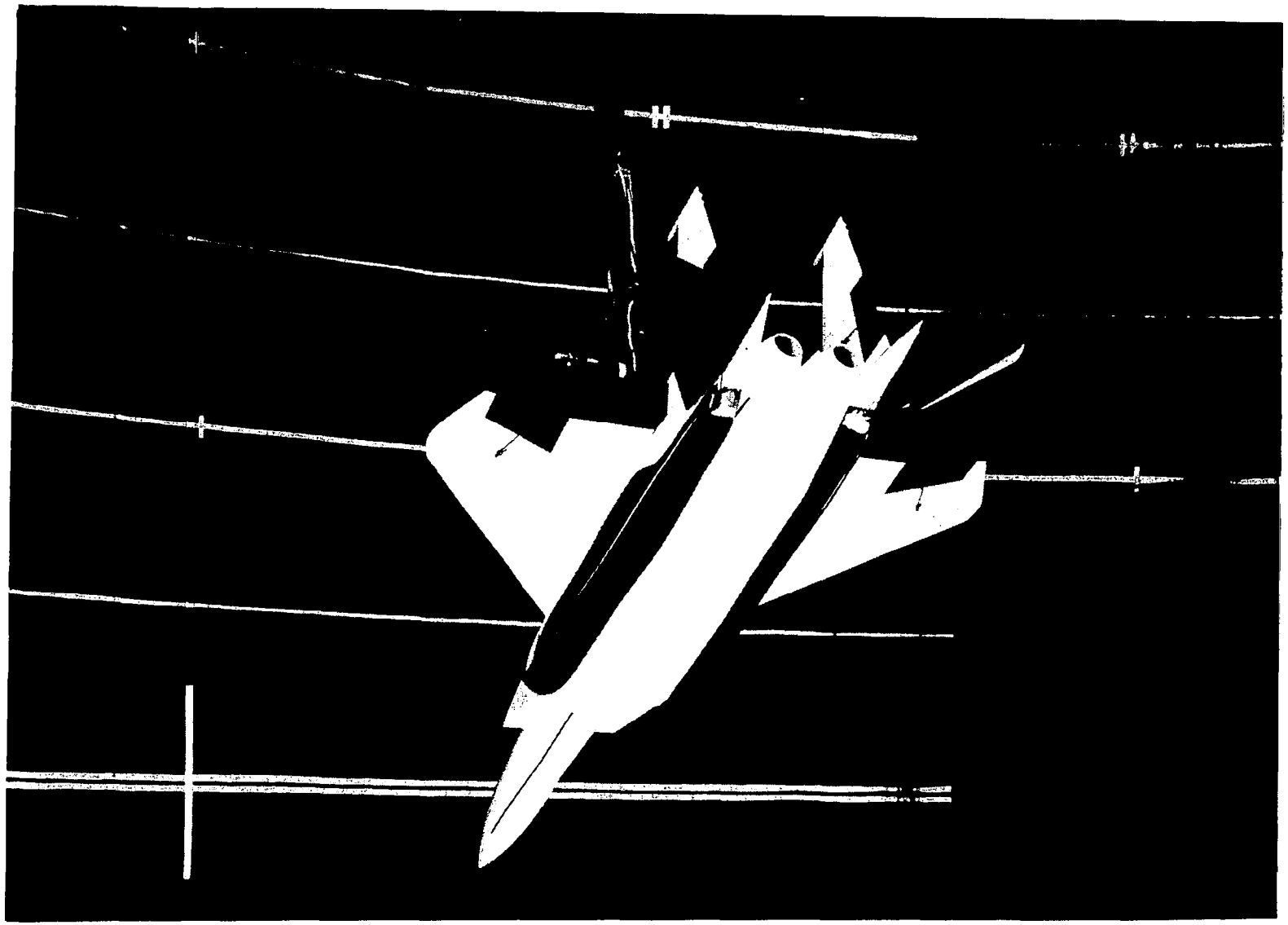

b) View from below model

Figure 1.- Concluded.

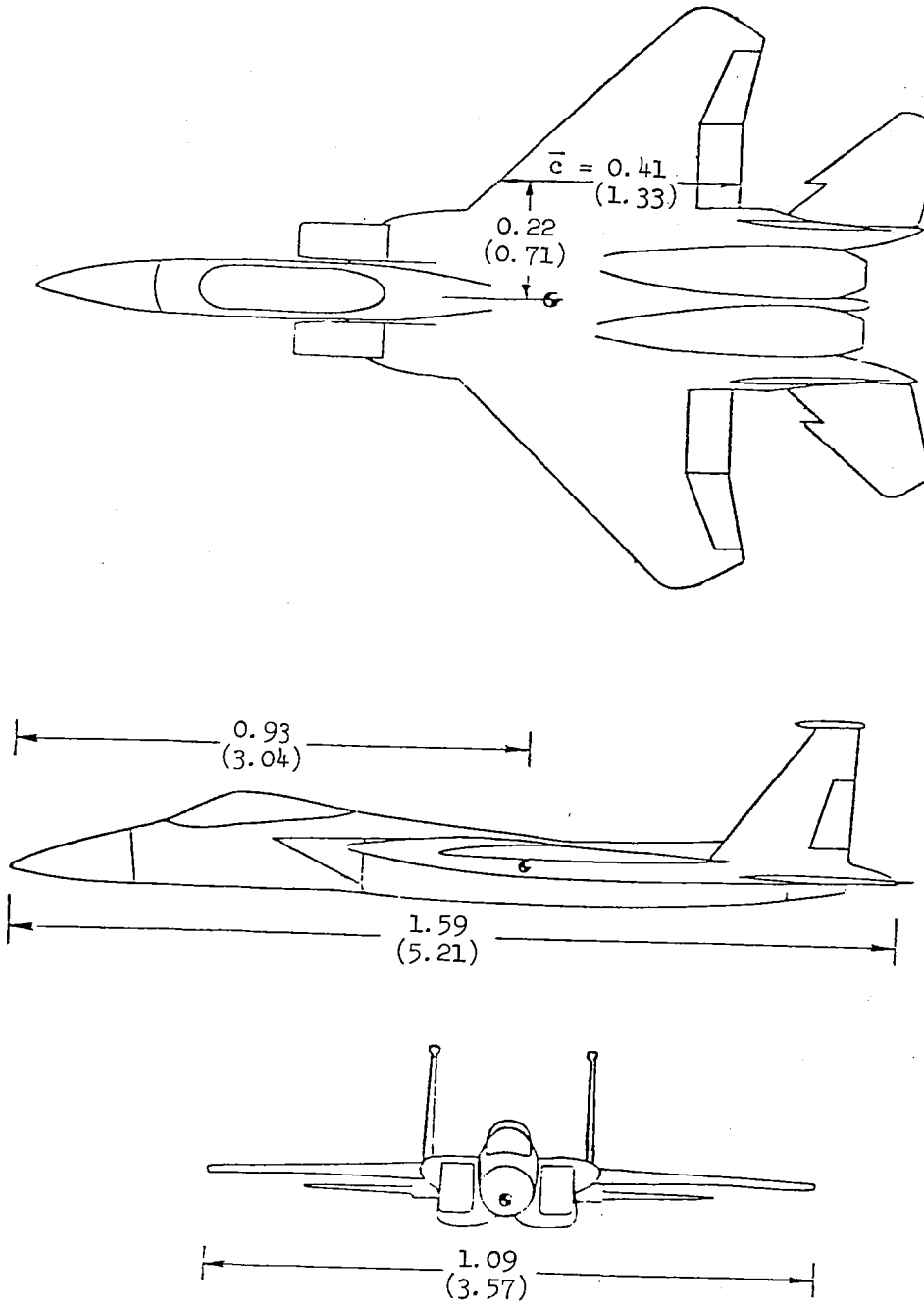

Figure 2.- Three-view sketch of 1/12-scale model.
(Dimensions are given in meters (feet).)

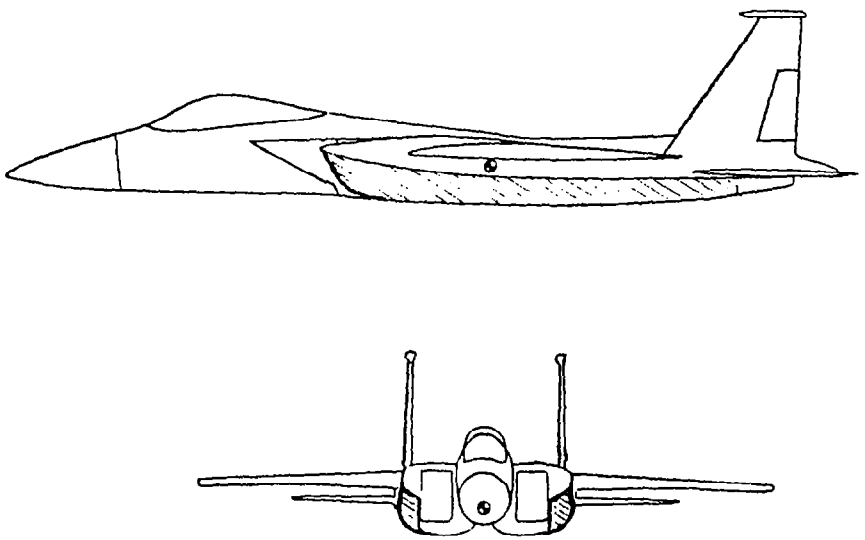

Figure 3.- Sketch of 1/12-scale model with conformal fuel tanks shown as shaded area.

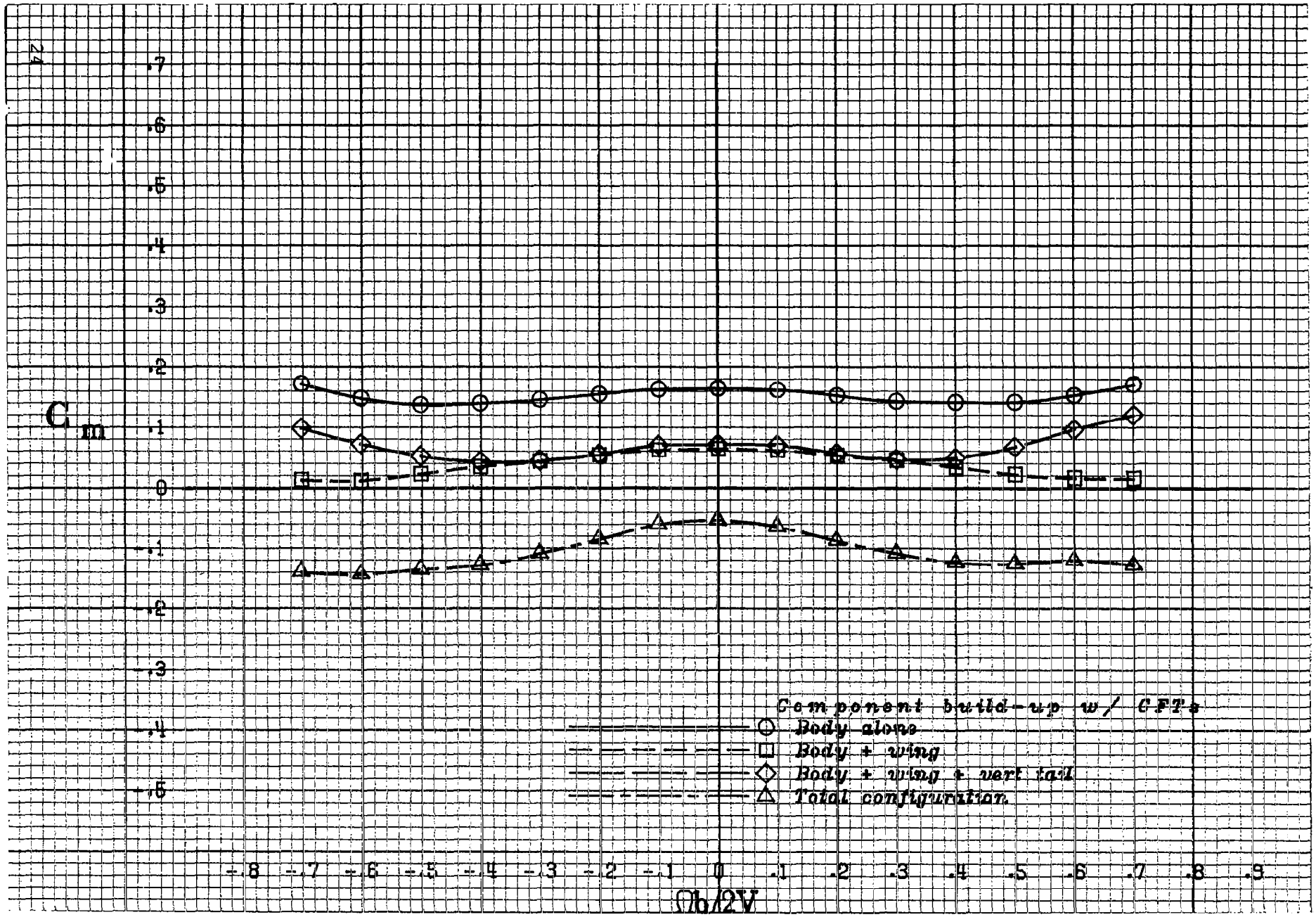

a) 20° angle of attack.

Figure 4.- Component build-up of the pitching-moment coefficient for the conformal fuel tank configured airplane.

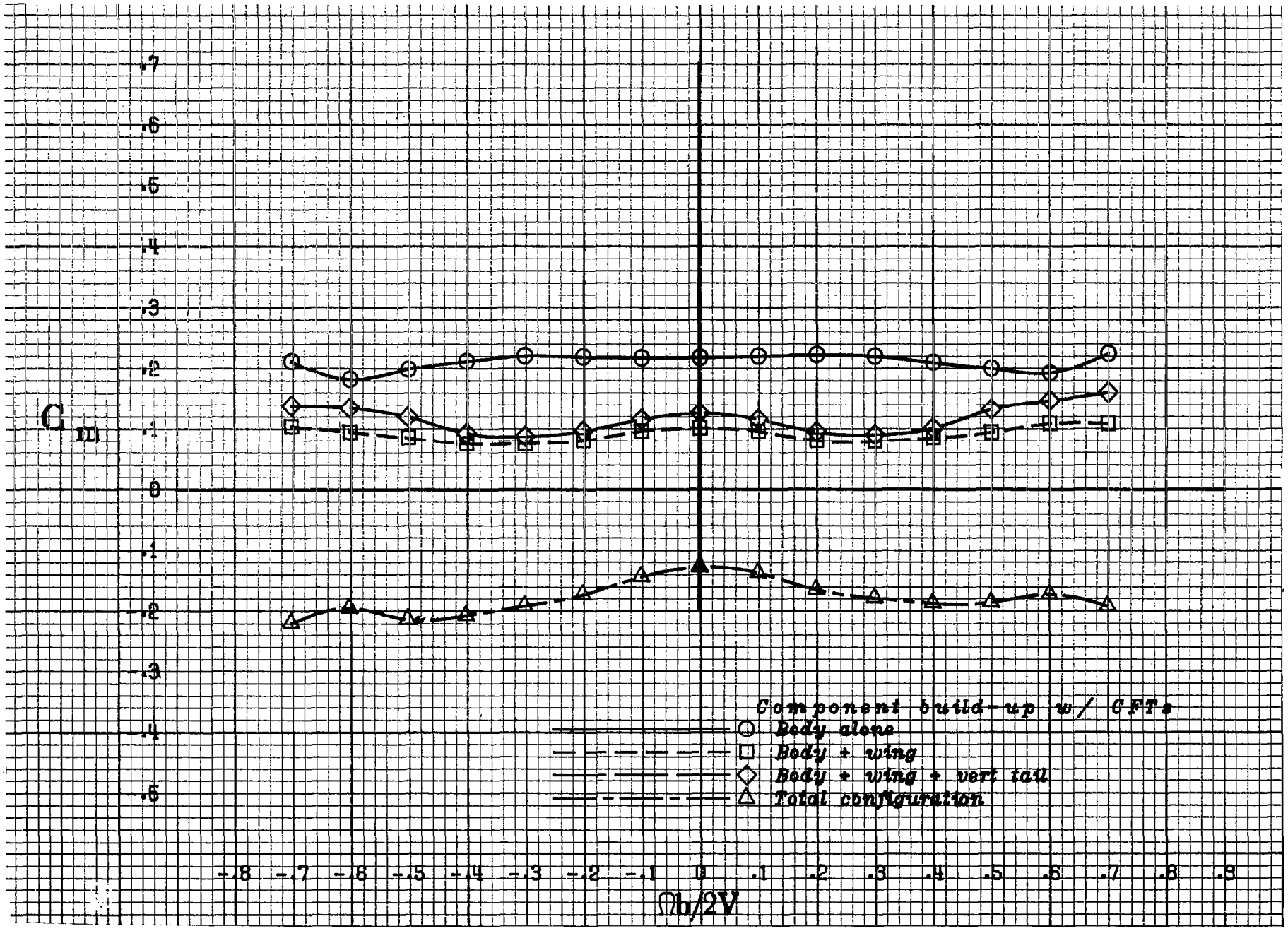

b) 30° angle of attack.

Figure 4.- Continued.

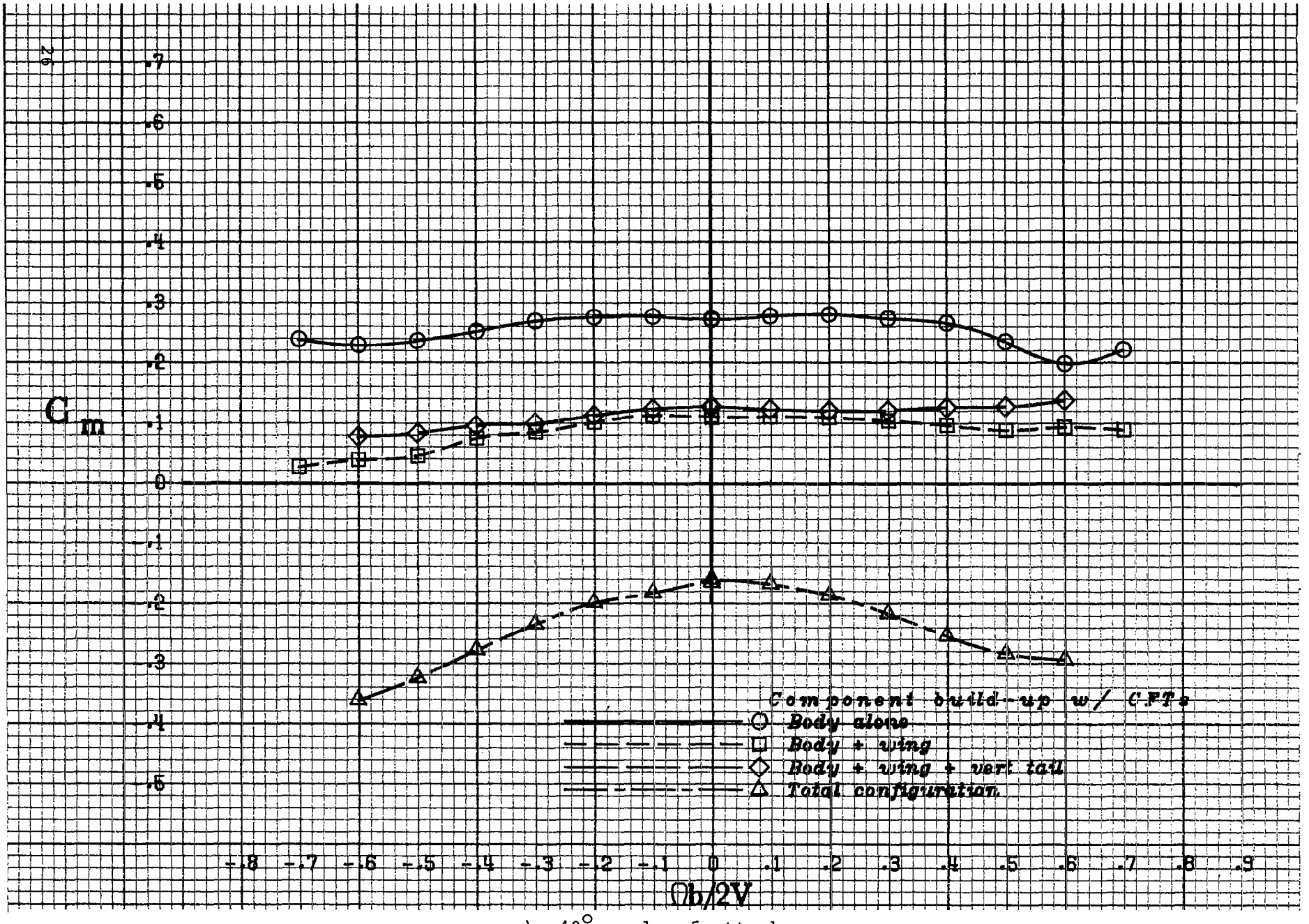

c) 40° angle of attack.

Figure 4.- Continued.

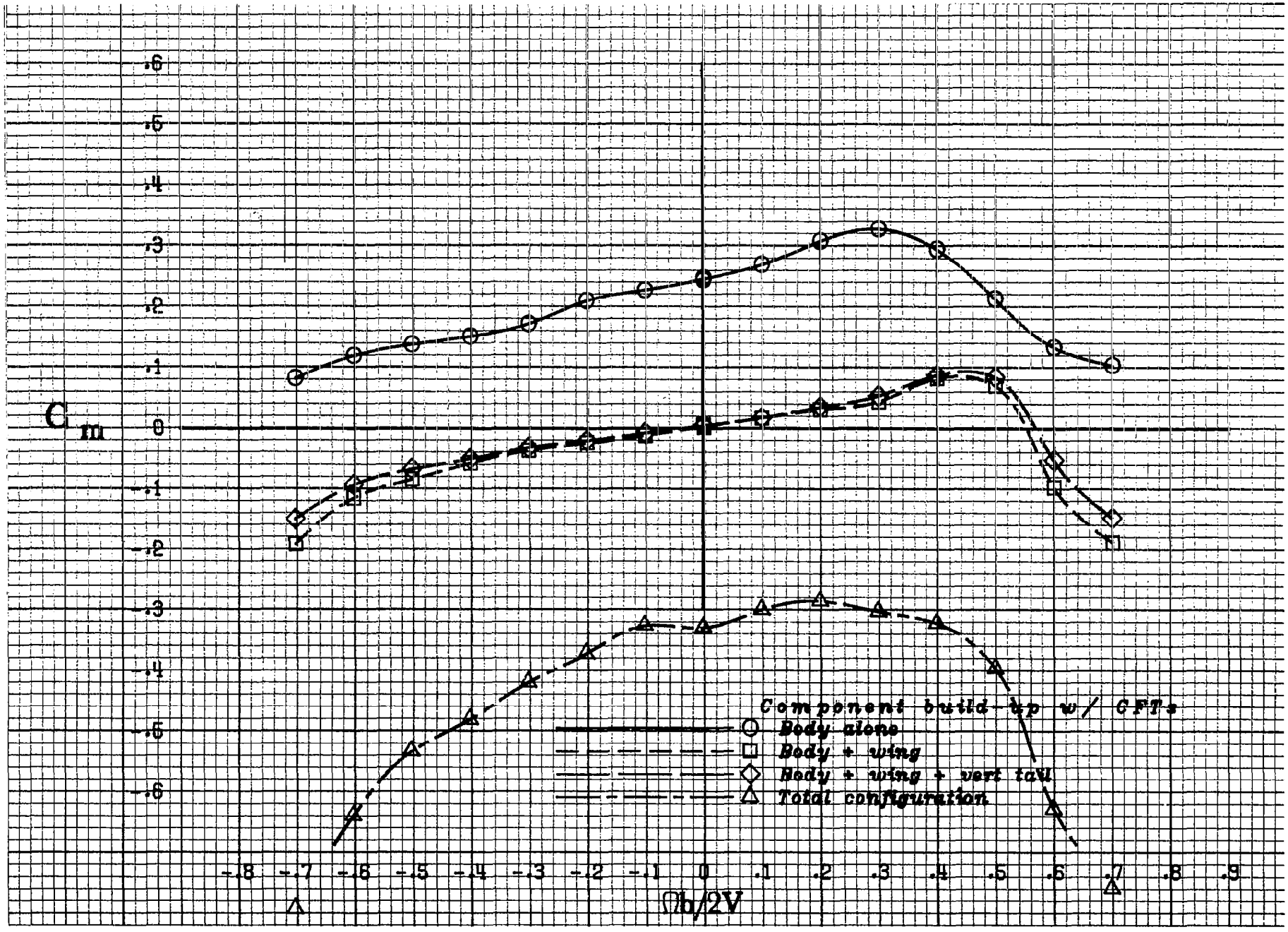

d) 60° angle of attack.

Figure 4.- Continued.

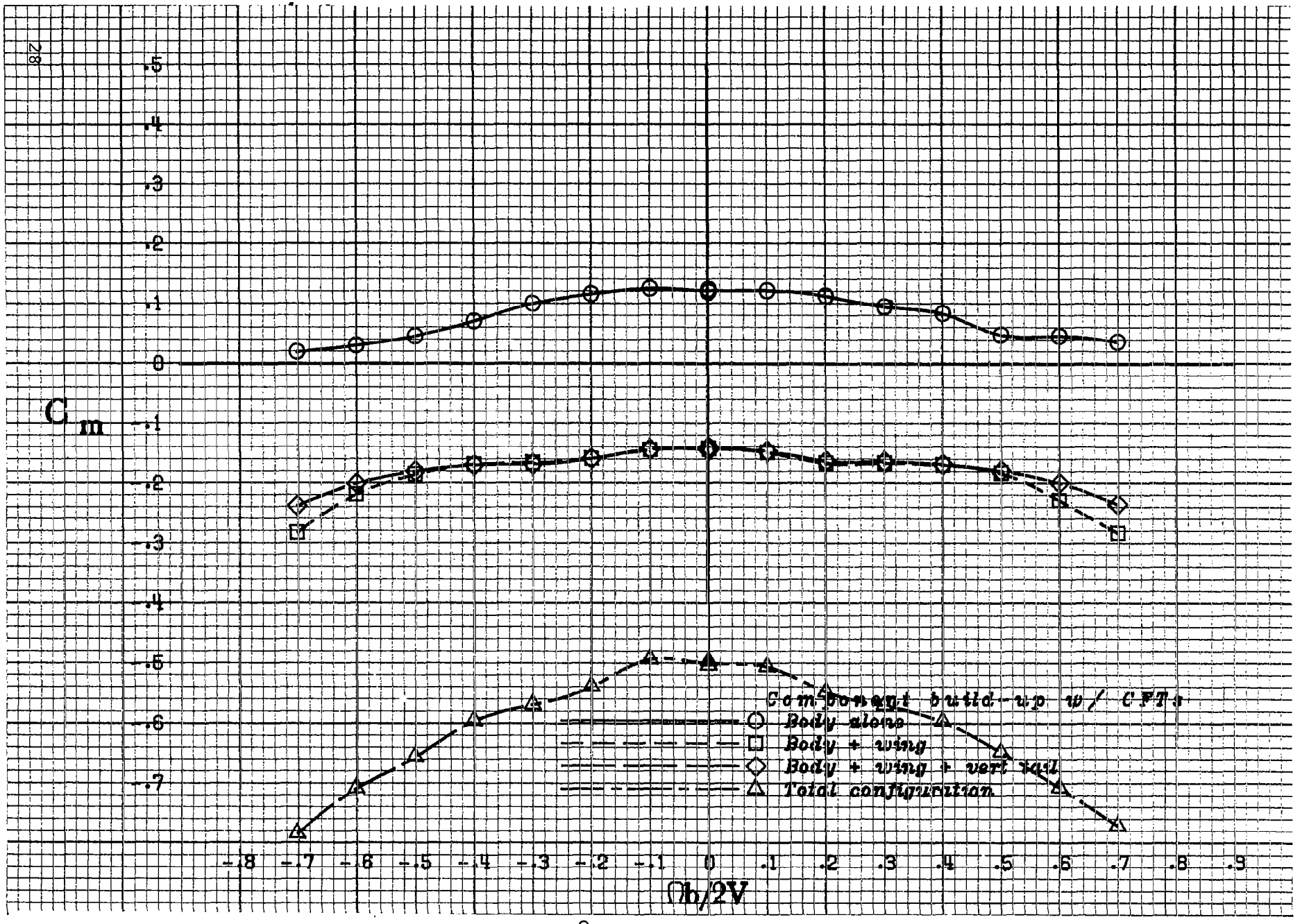

e) 80° angle of attack.

Figure 4.- Concluded.

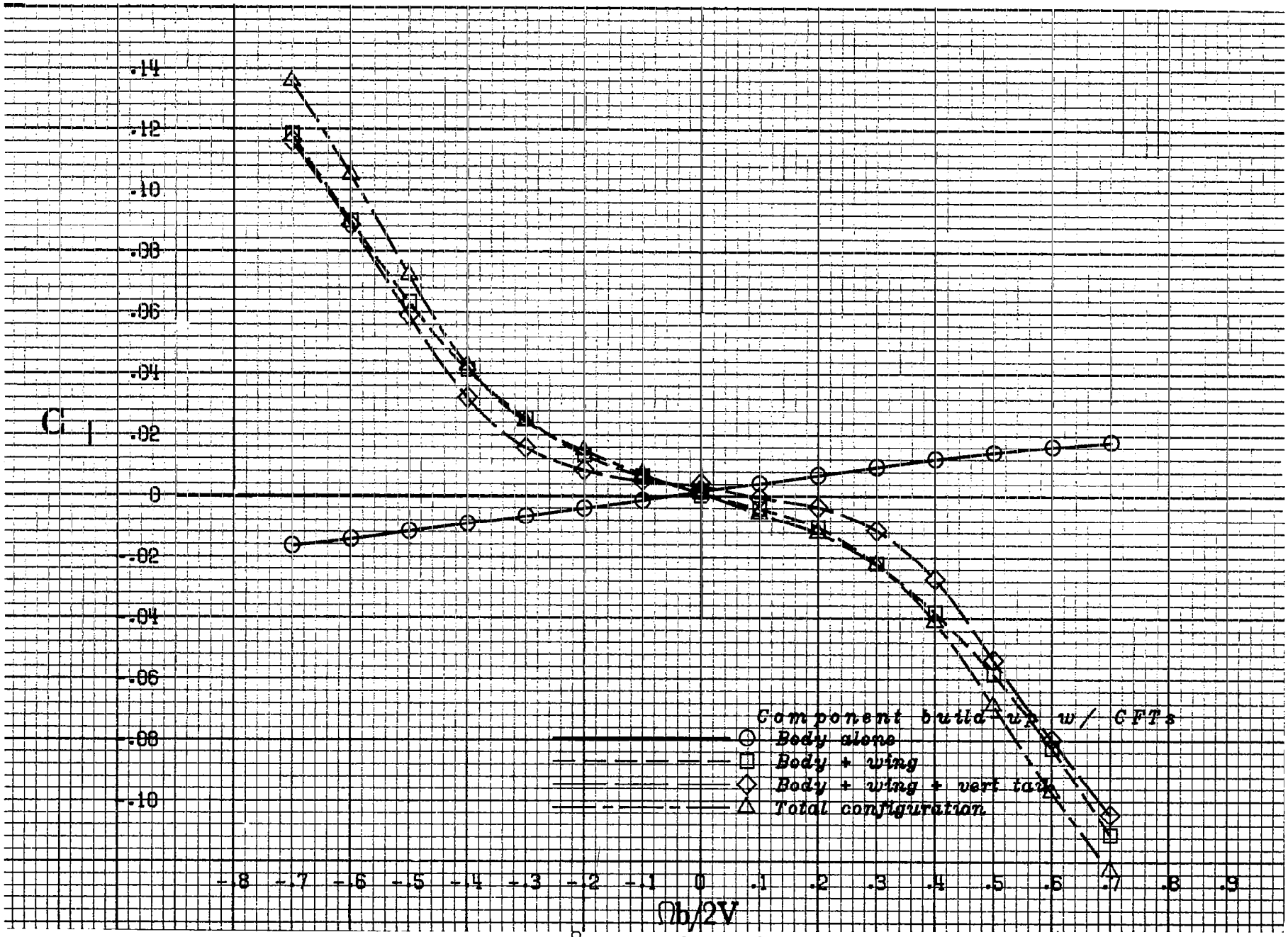

a) 20° angle of attack.

Figure 5.- Component build-up of the rolling-moment coefficient for the conformal fuel tank configured airplane.

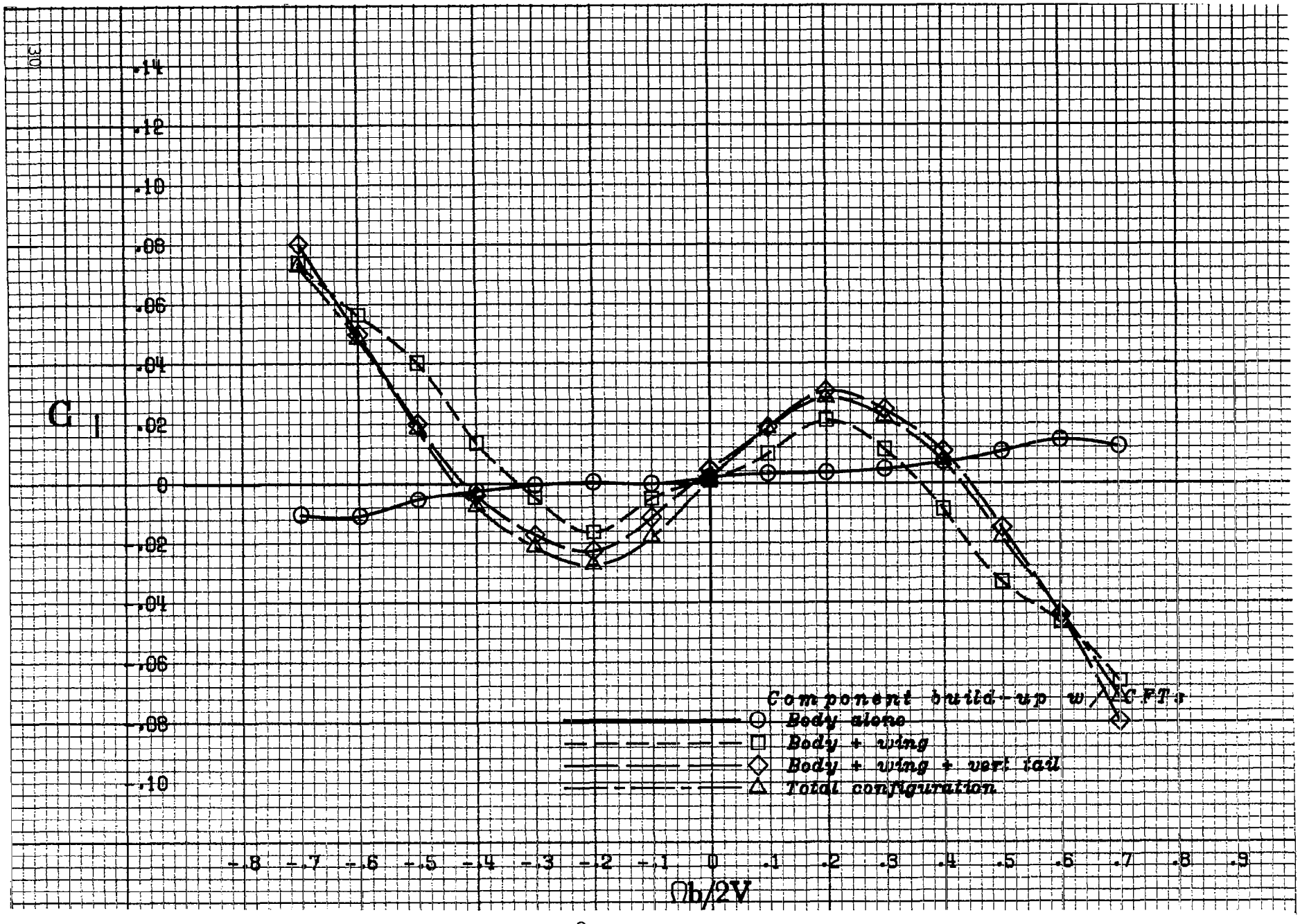

b) 30° angle of attack.

Figure 5.- Continued.

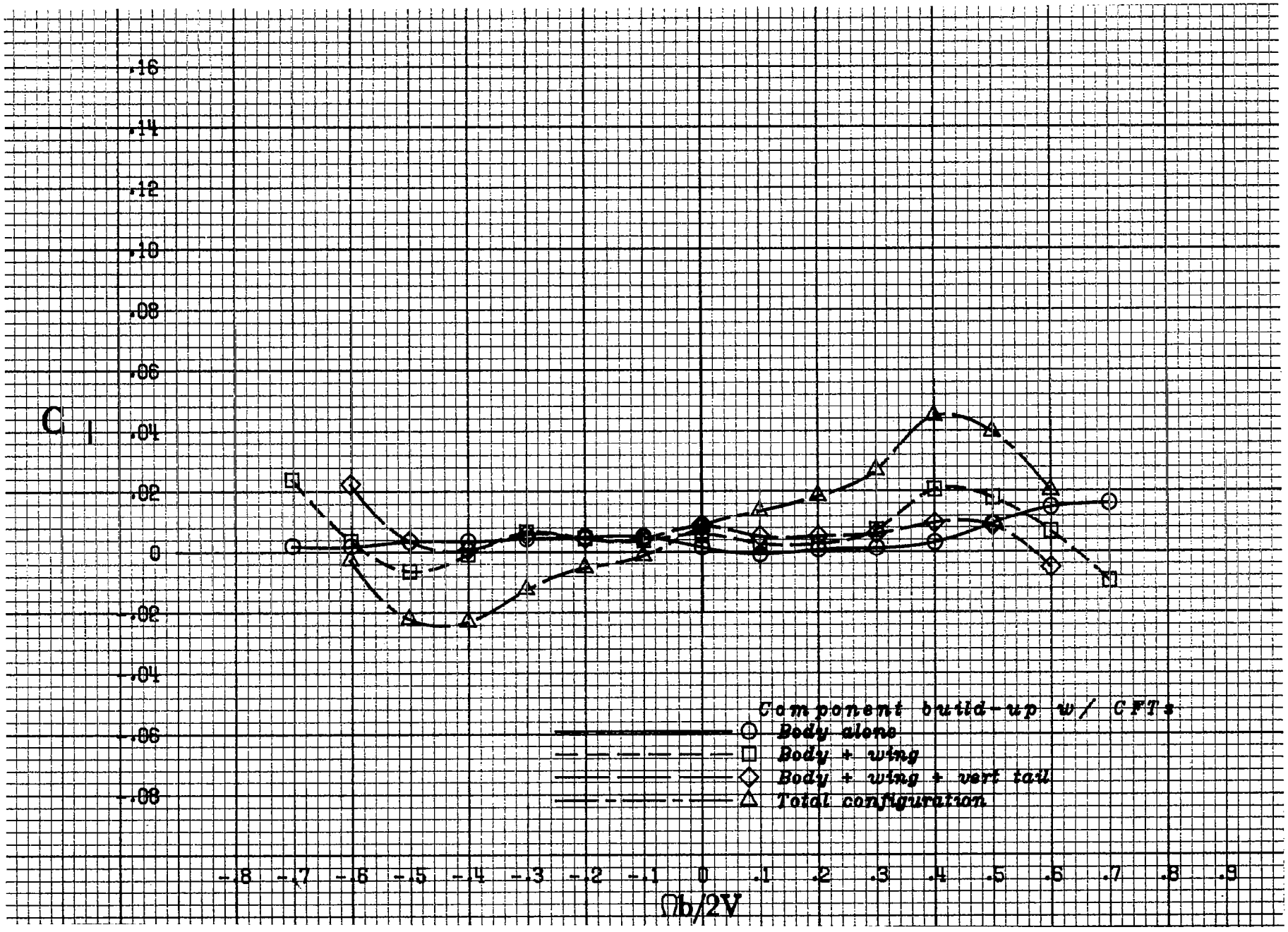

c) 40° angle of attack.

Figure 5.- Continued.

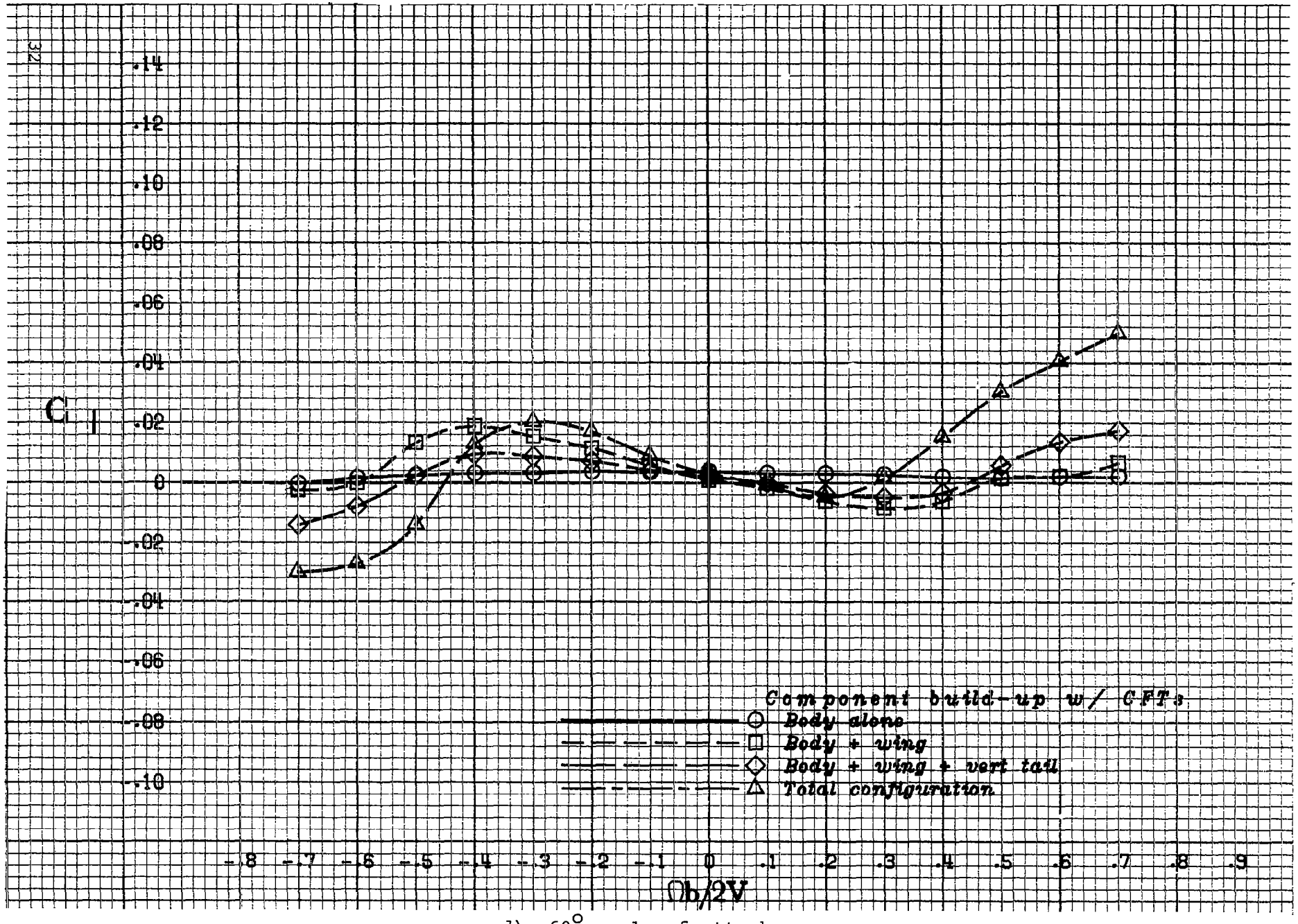

d) 60^{o} angle of attack.

Figure 5.- Continued.

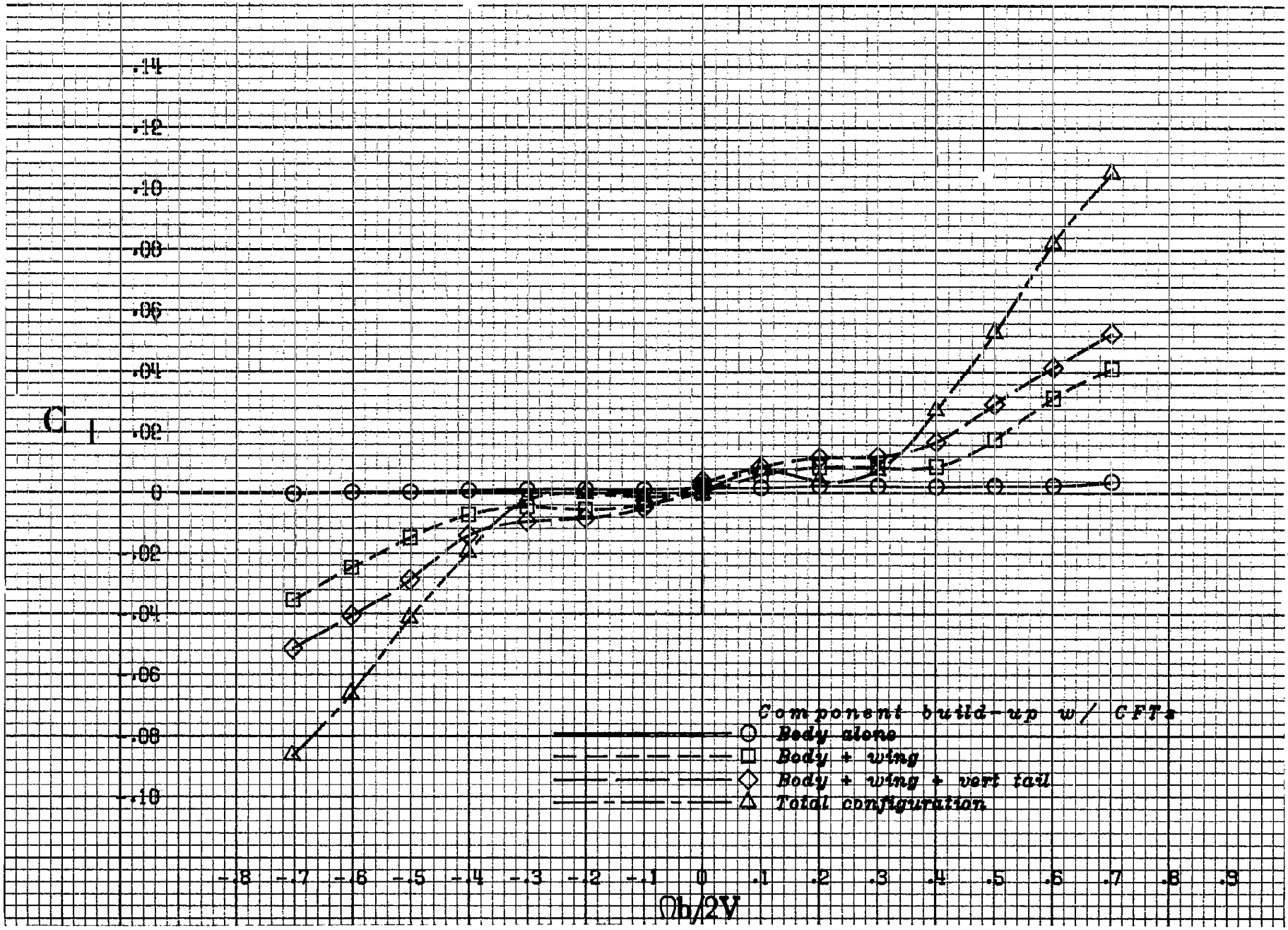

e) 80° angle of attack.

Figure 5.- Concluded.

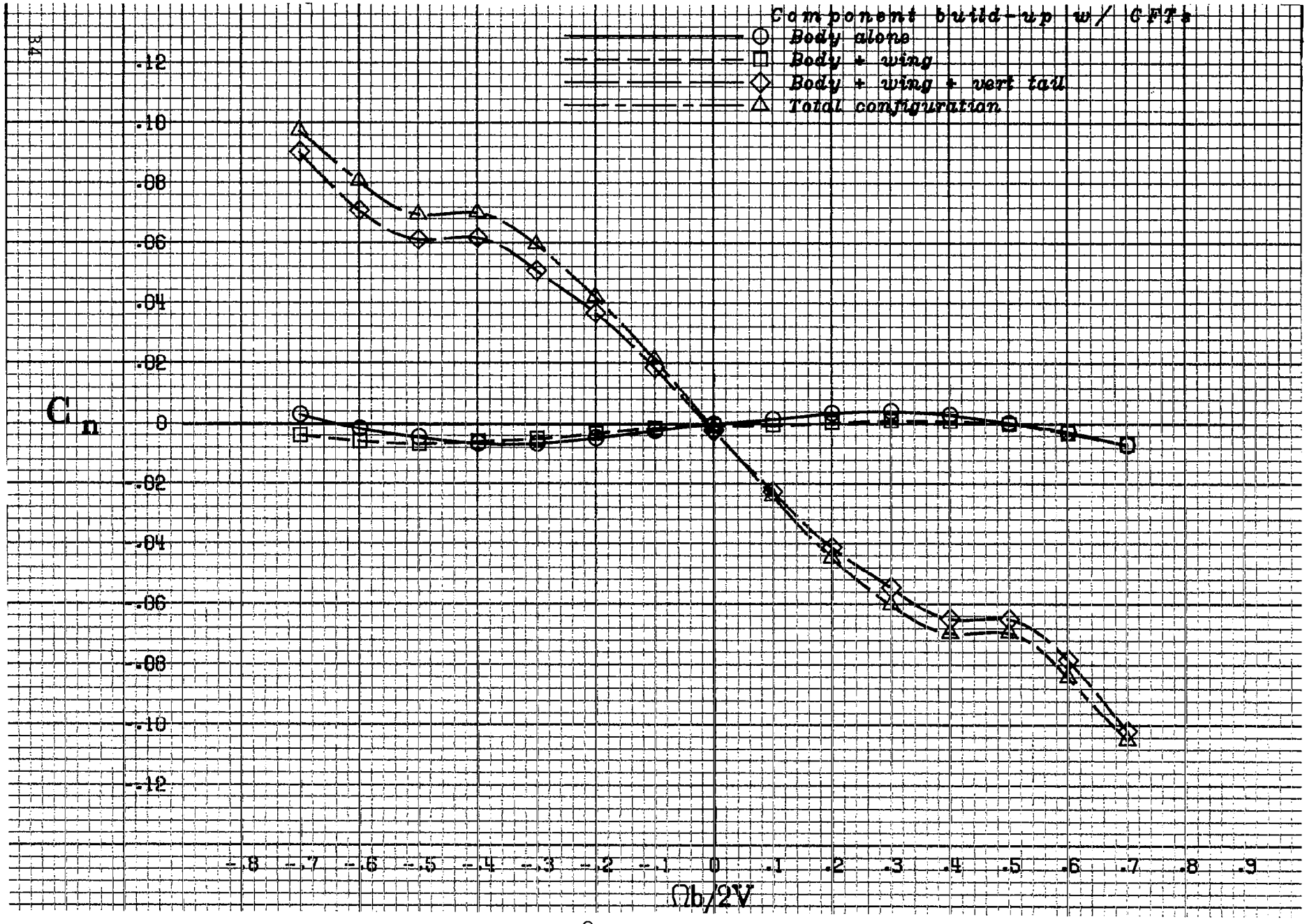

a) 20° angle of attack.

Figure 6.- Component build-up of the yawing-moment coefficient for the conformal fuel tank configured airplane.

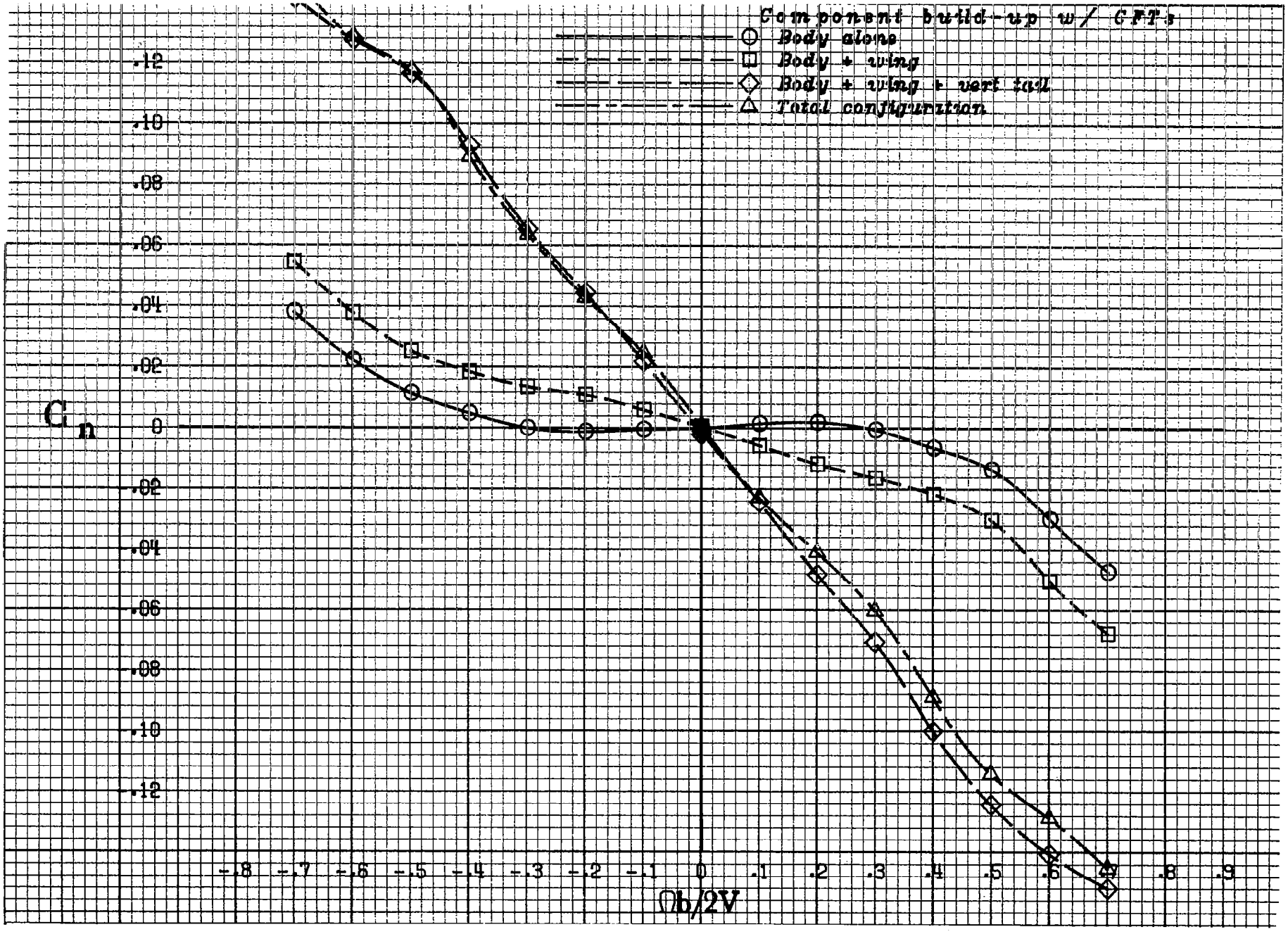

b) 30° angle of attack.

Figure 6.- Continued.

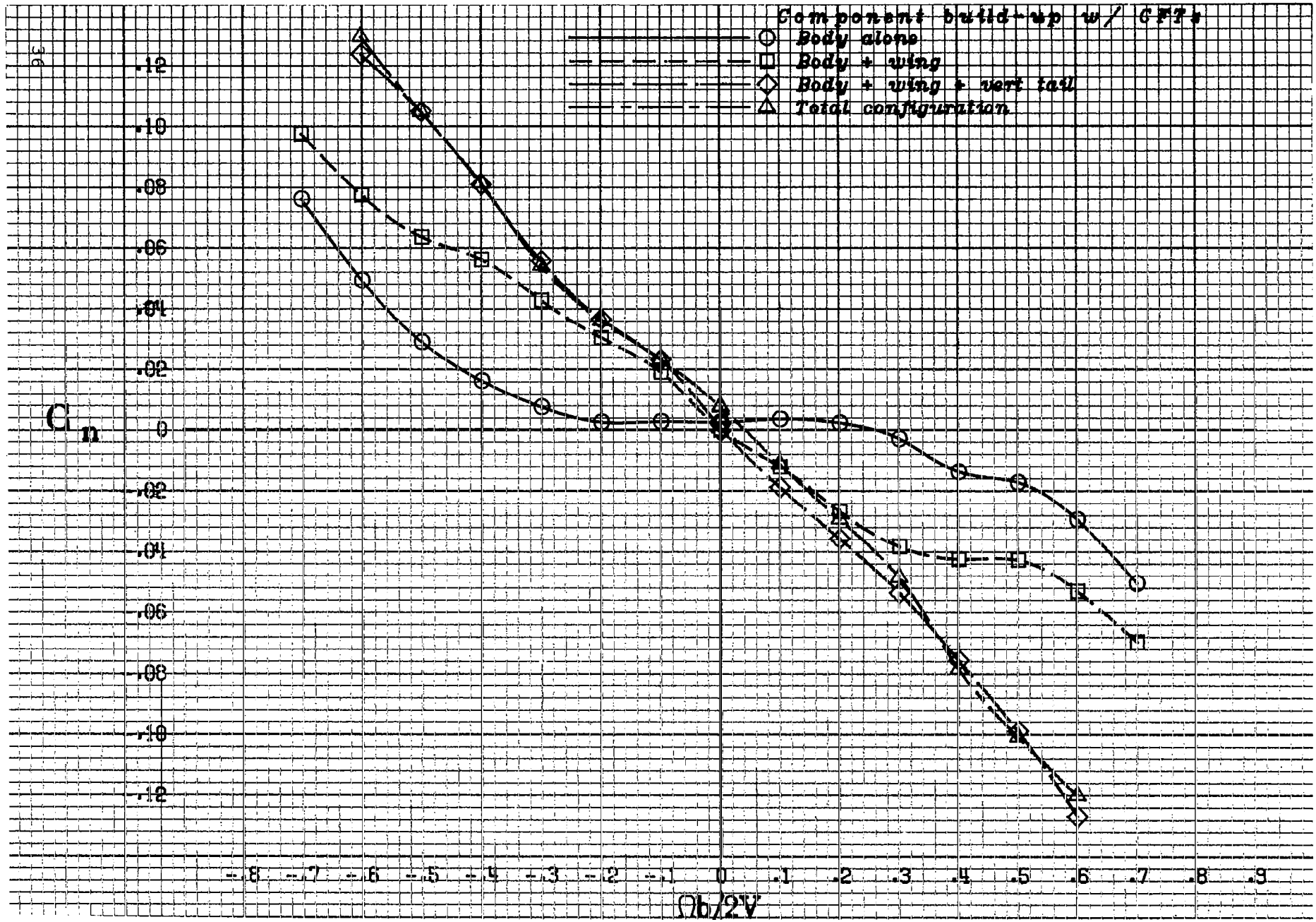

c) 40° angle of attack.

Figure 6.- Continued.

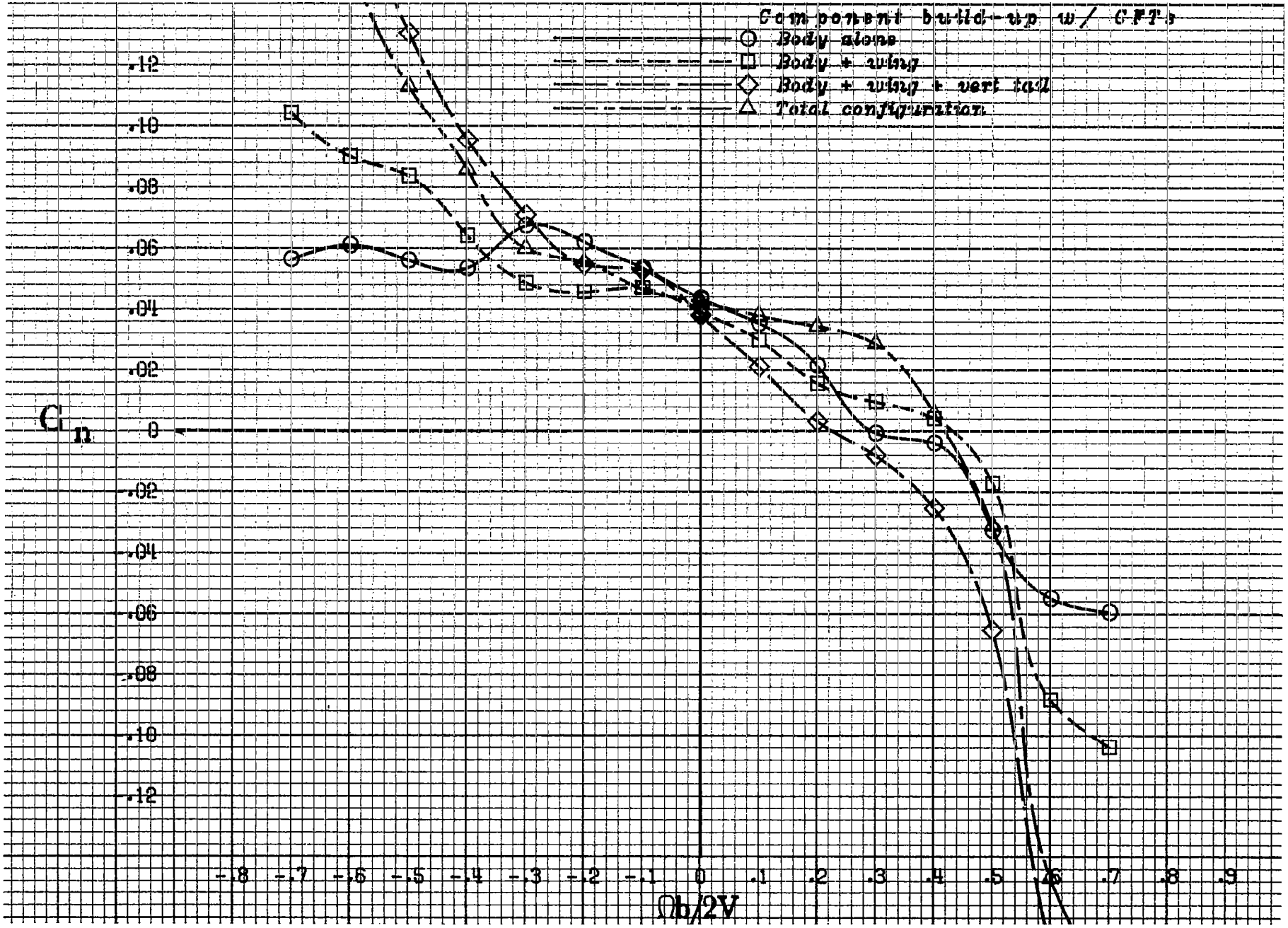

d) 60° angle of attack.

Figure 6.- Continued.

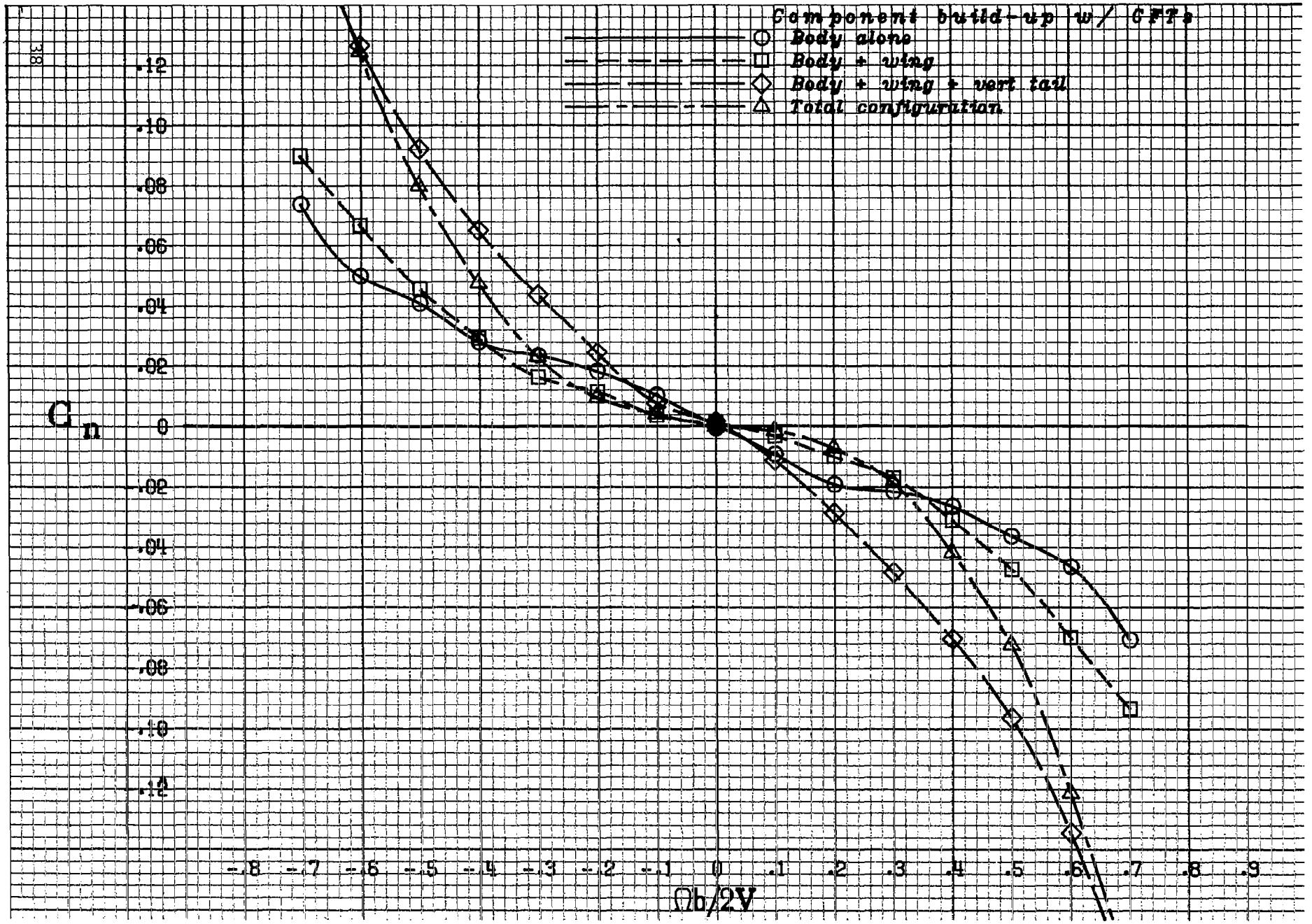

e) 80° angle of attack.

Figure 6.- Concluded.

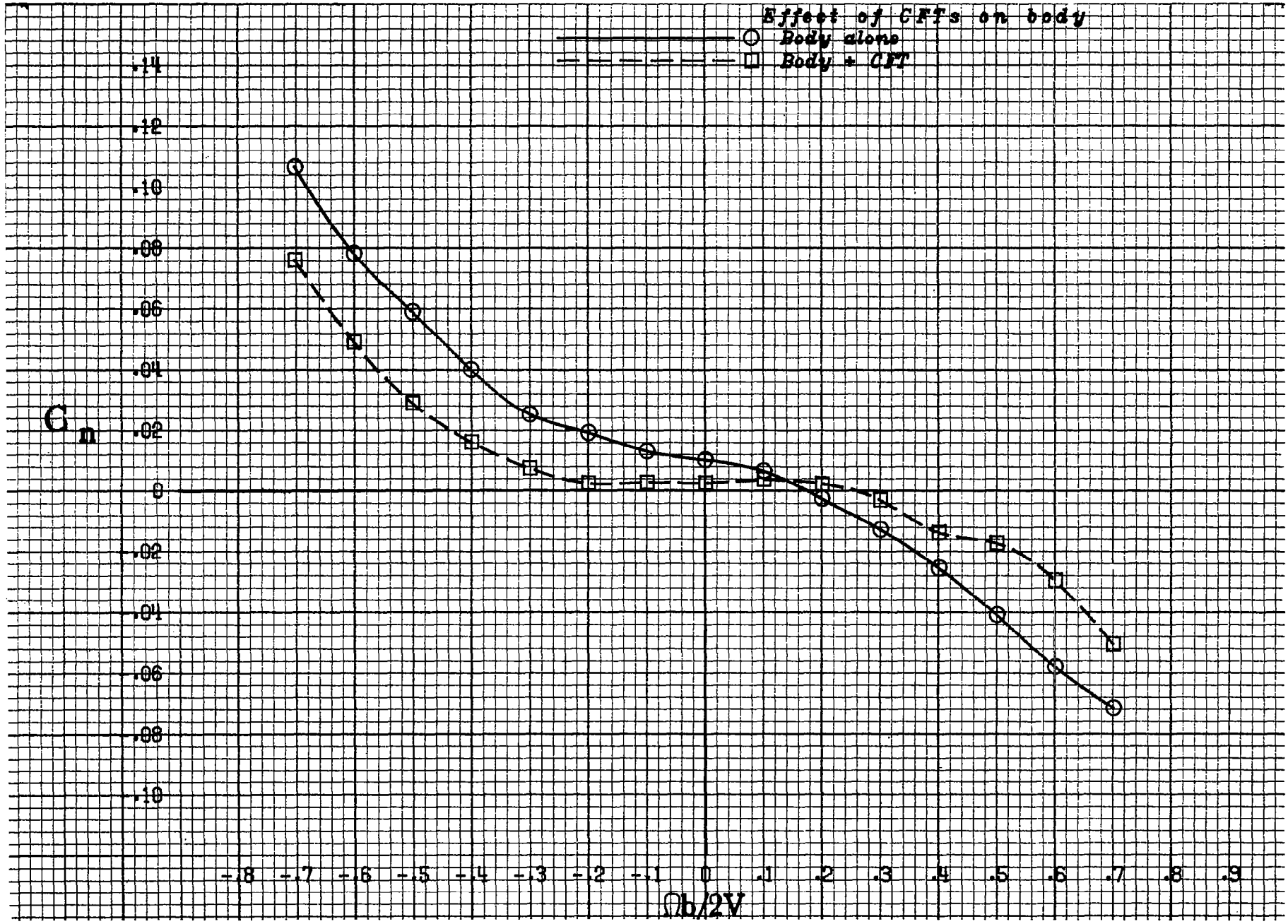

a) 40° angle of attack.

Figure 7.- Effect of adding conformal fuel tanks on the yawing-moment coefficient for the body alone.

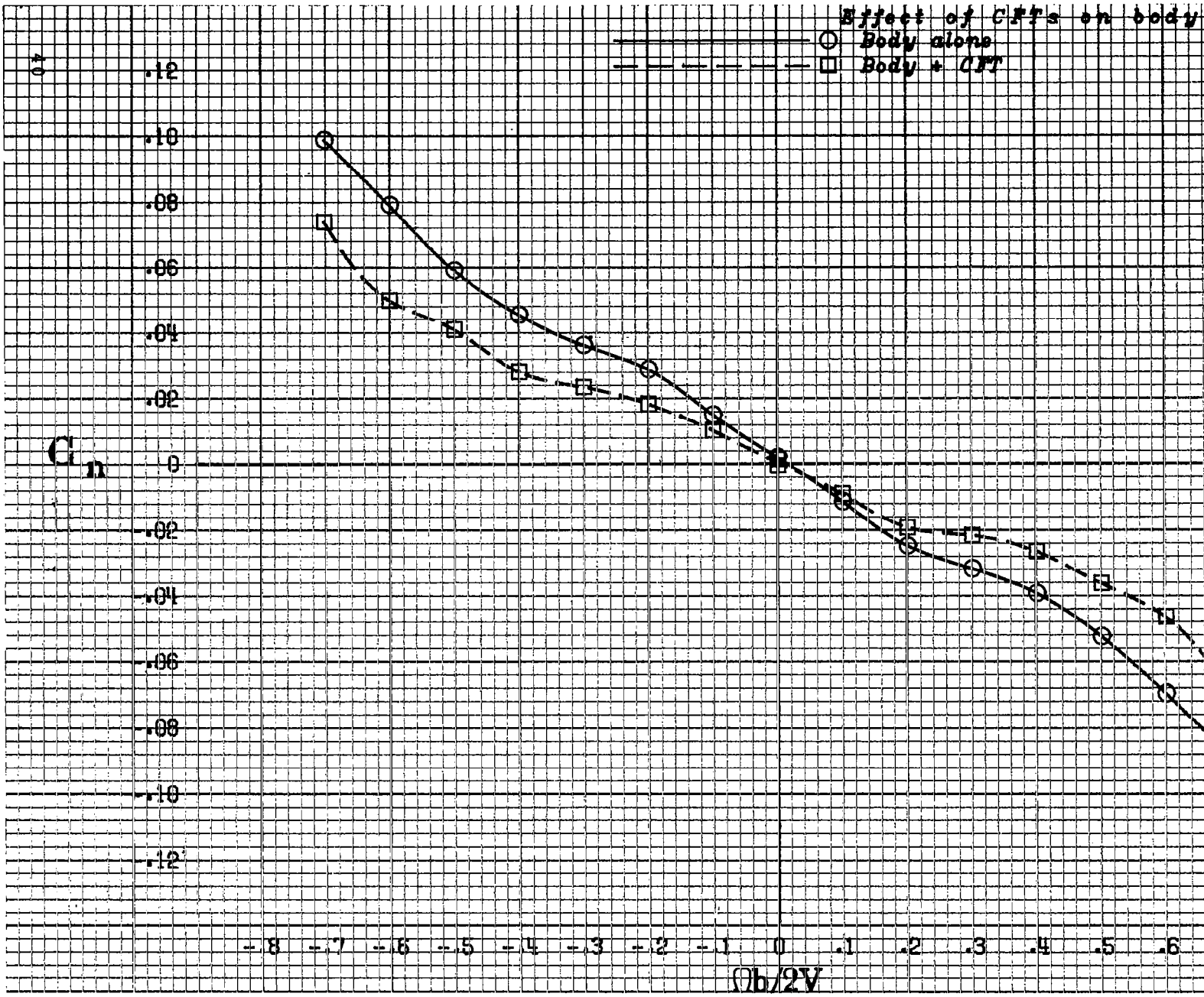

b) 80° angle of attack.

Figure 7.- Concluded.

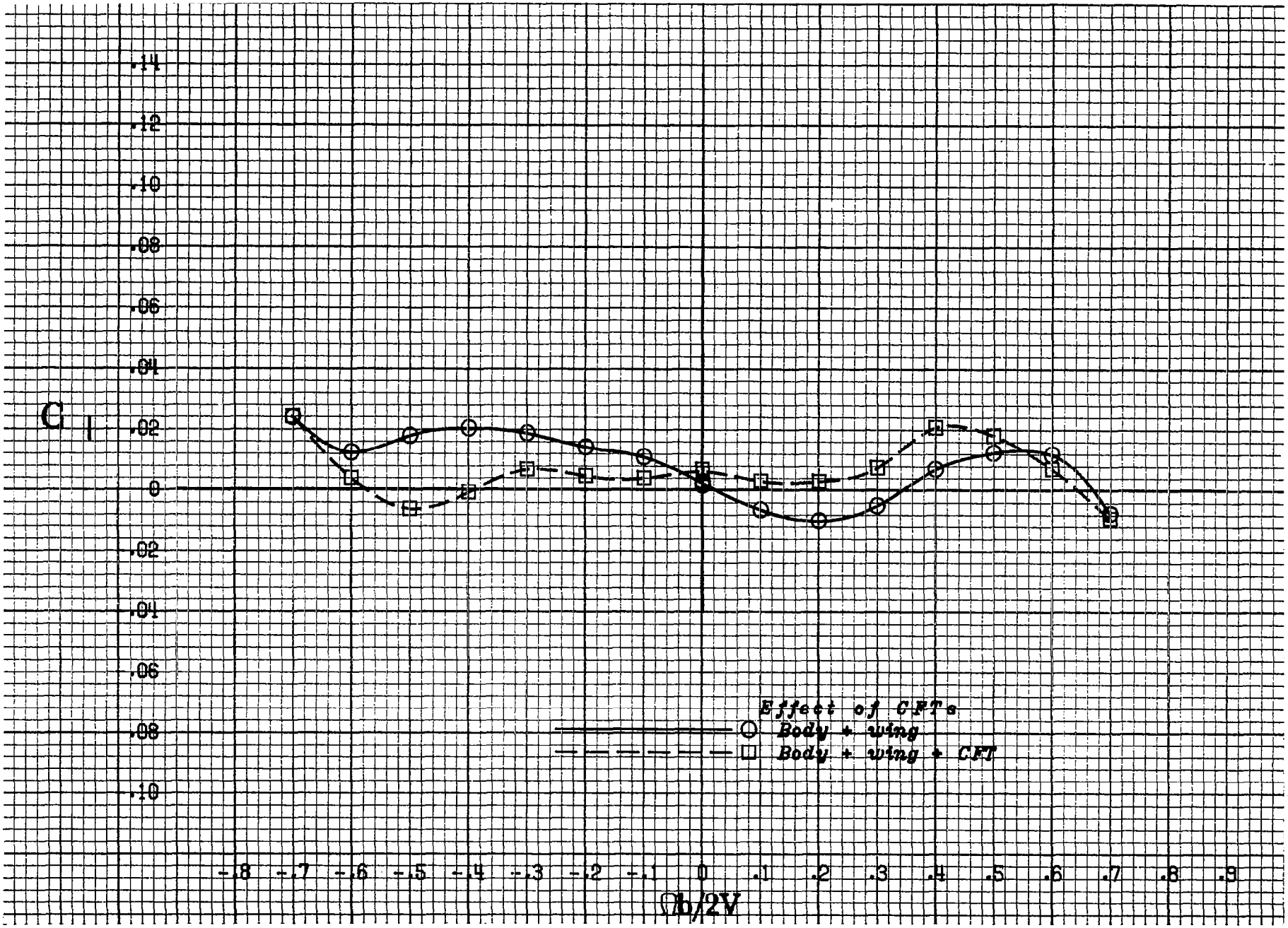

Figure 8.- Effect of adding conformal fuel tanks on the rolling-moment coefficient for the body + wing at 40° angle of attack.

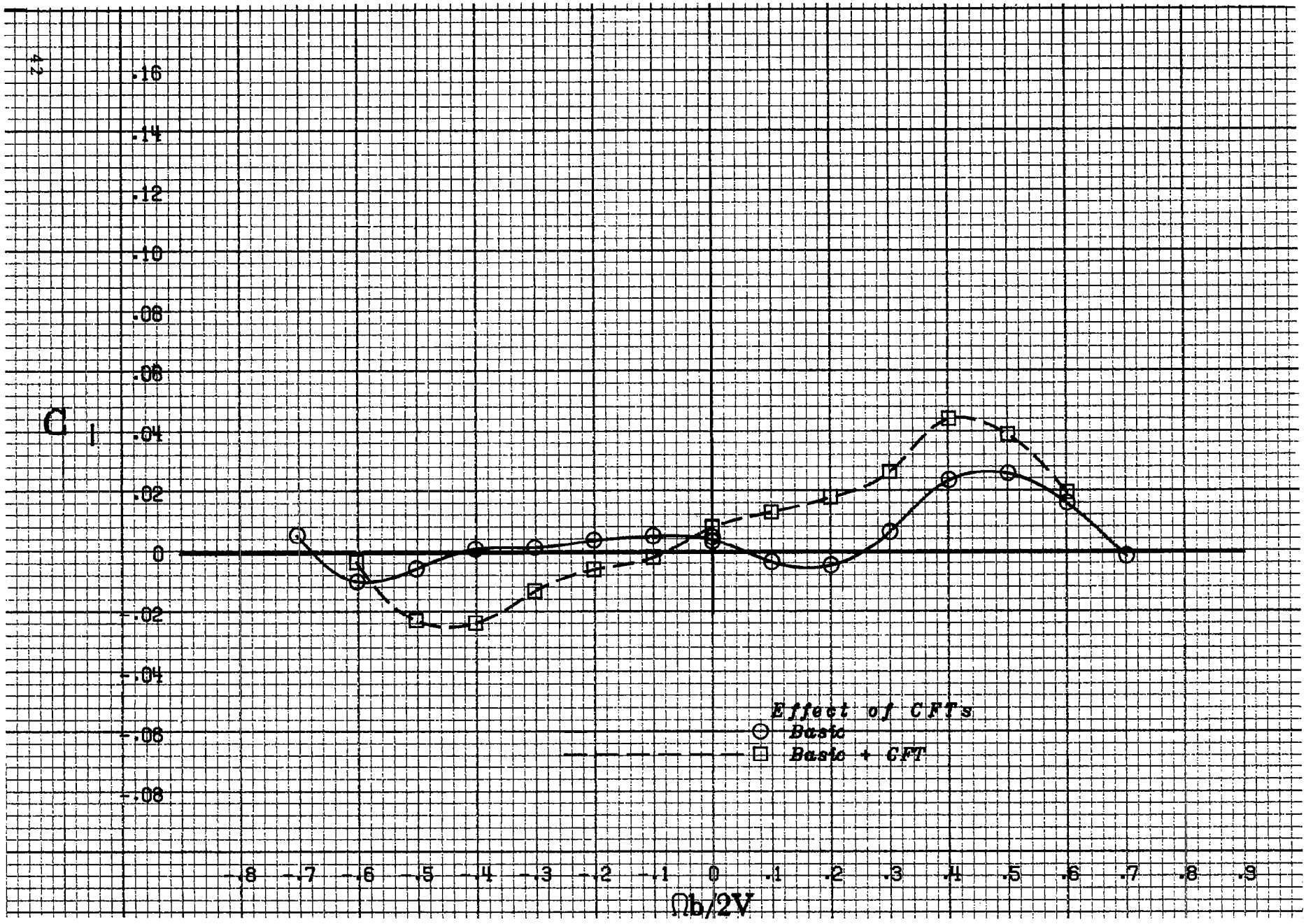

Figure 9.- Effect of adding conformal fuel tanks on the rolling-moment coefficient for the basic airplane with neutral controls. 40° angle of attack.

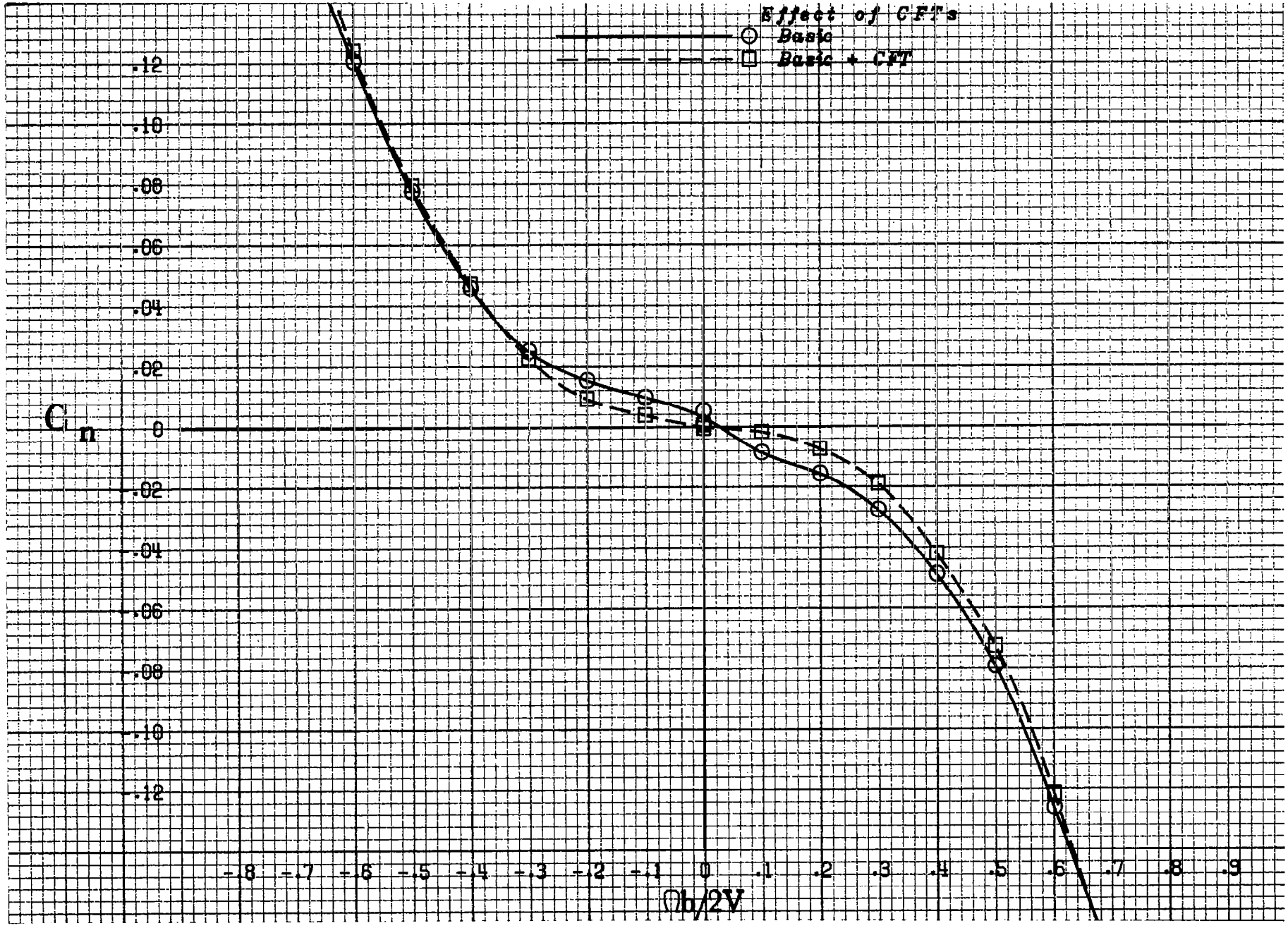

Figure 10.- Effect of adding conformal fuel tanks on the yawing-moment coefficient for the basic airplane with neutral controls. 80° angle of attack.

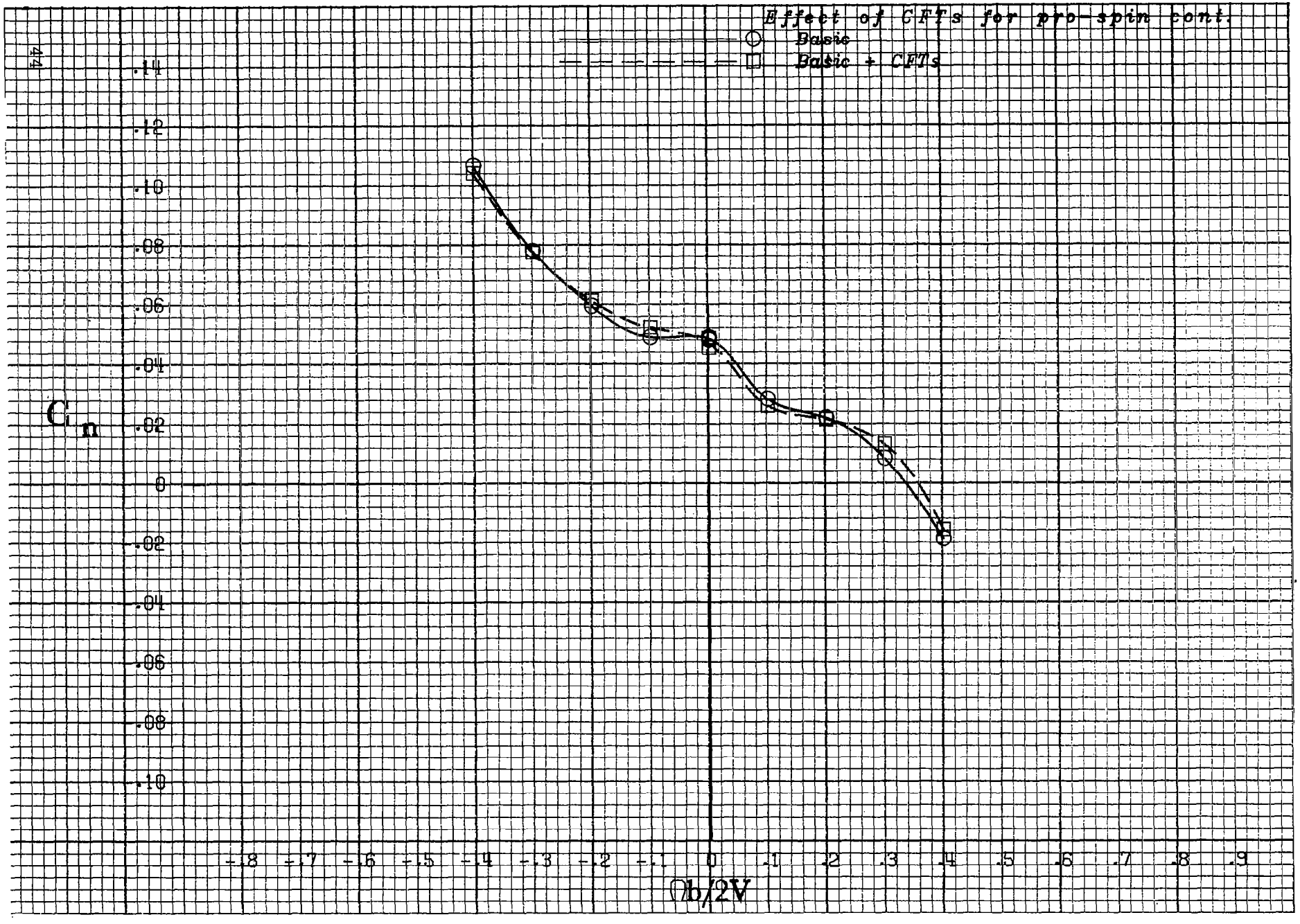

a) 50° angle of attack.

Figure 11.- Effect of adding conformal fuel tanks on the yawing-moment coefficient for the basic airplane with right pro-spin controls. $\delta_e=0$; $\delta_d=6^{\circ}$; $\delta_a=20^{\circ}$; $\delta_r=-15^{\circ}$.

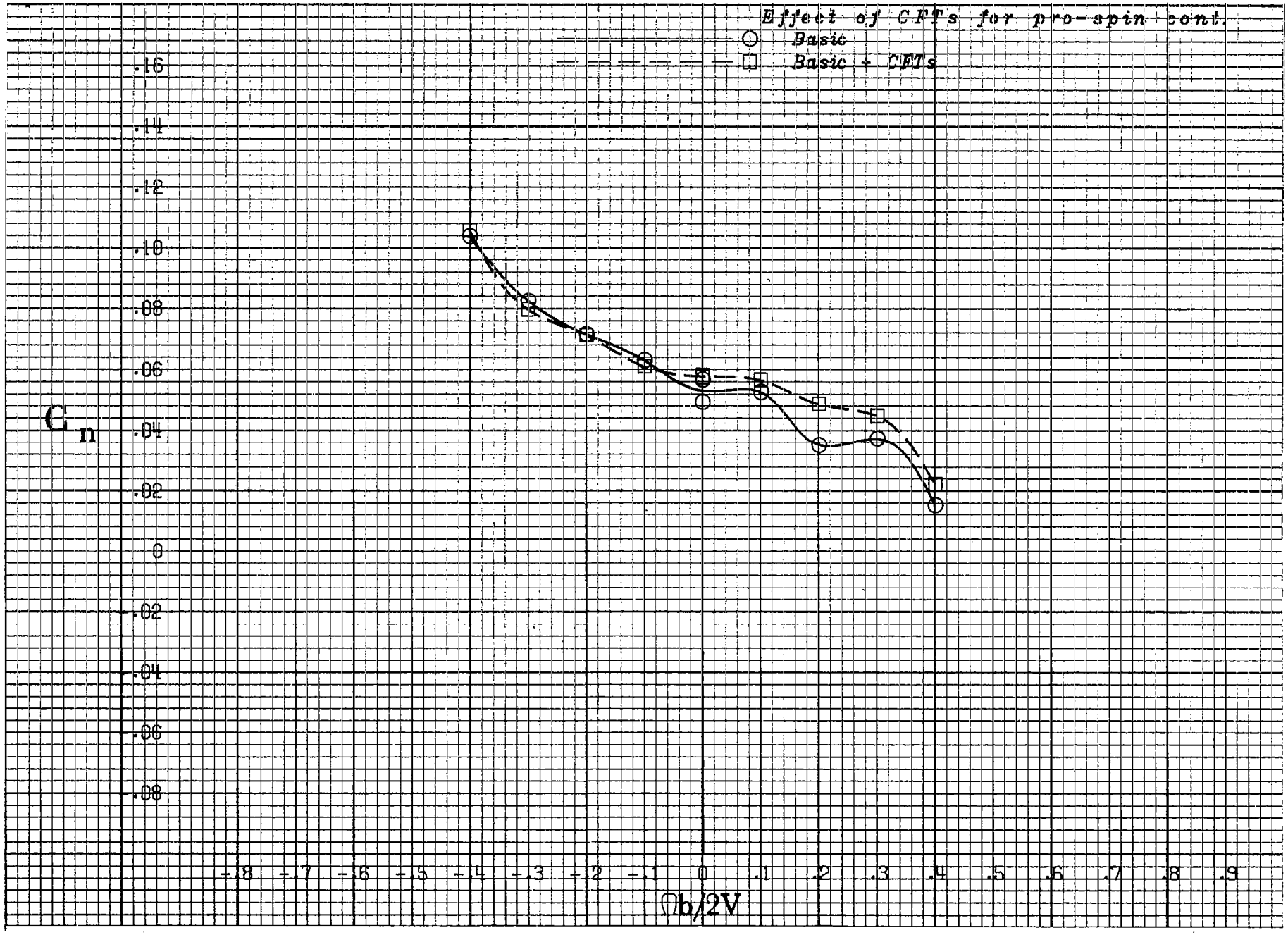

b) 60^{o} angle of attack.

Figure 11.- Continued.

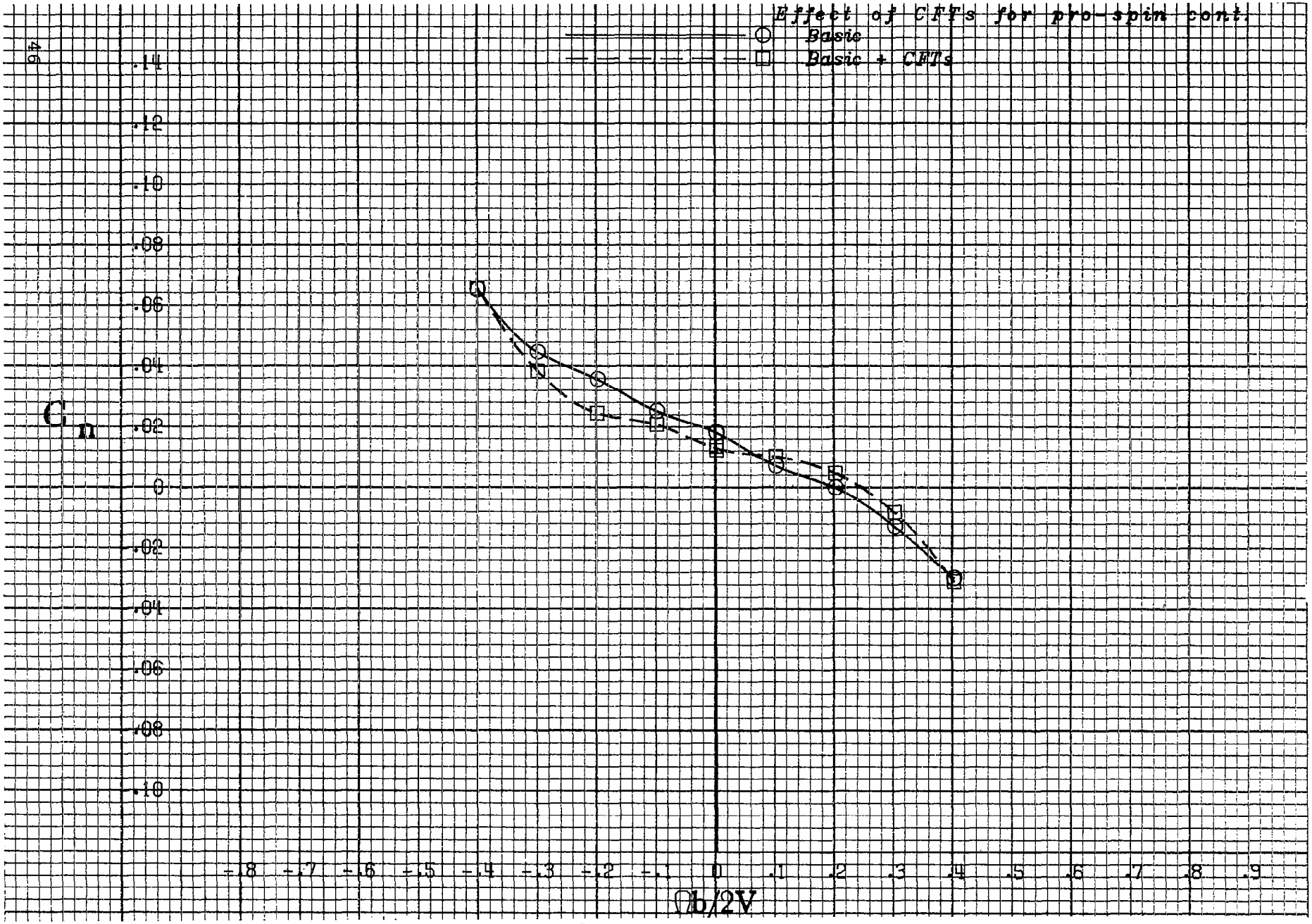

c) 80° angle of attack.

Figure 11.- Concluded.

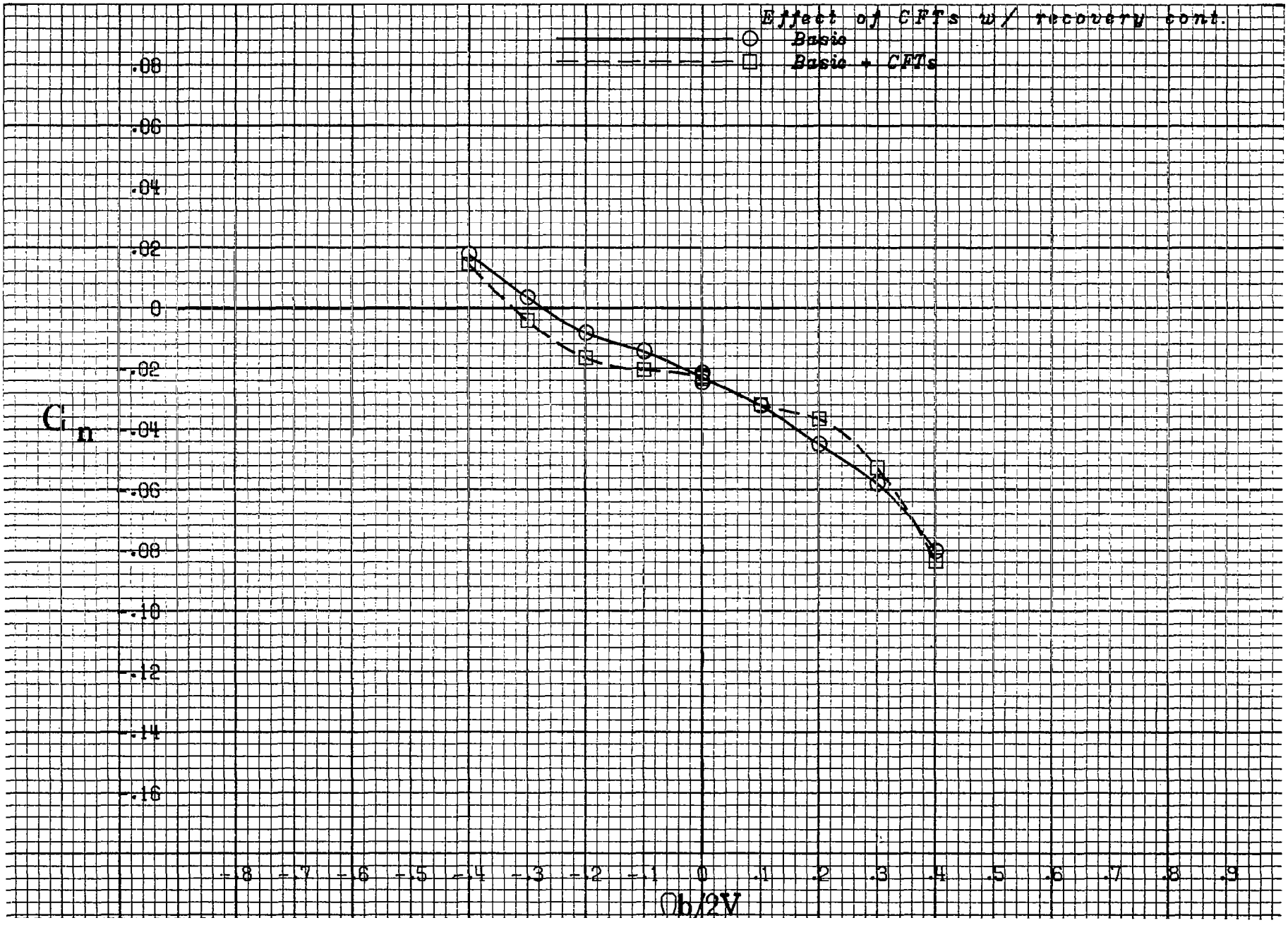

a) 80^{o} angle of attack.

Figure 12.- Effect of adding conformal fuel tanks on the yawing-moment coefficient for the basic airplane with right recovery controls. $\delta_e=0$; $\delta_d= -6^{o}$; $\delta_a= -20^{o}$; $\delta_r=30^{o}$.

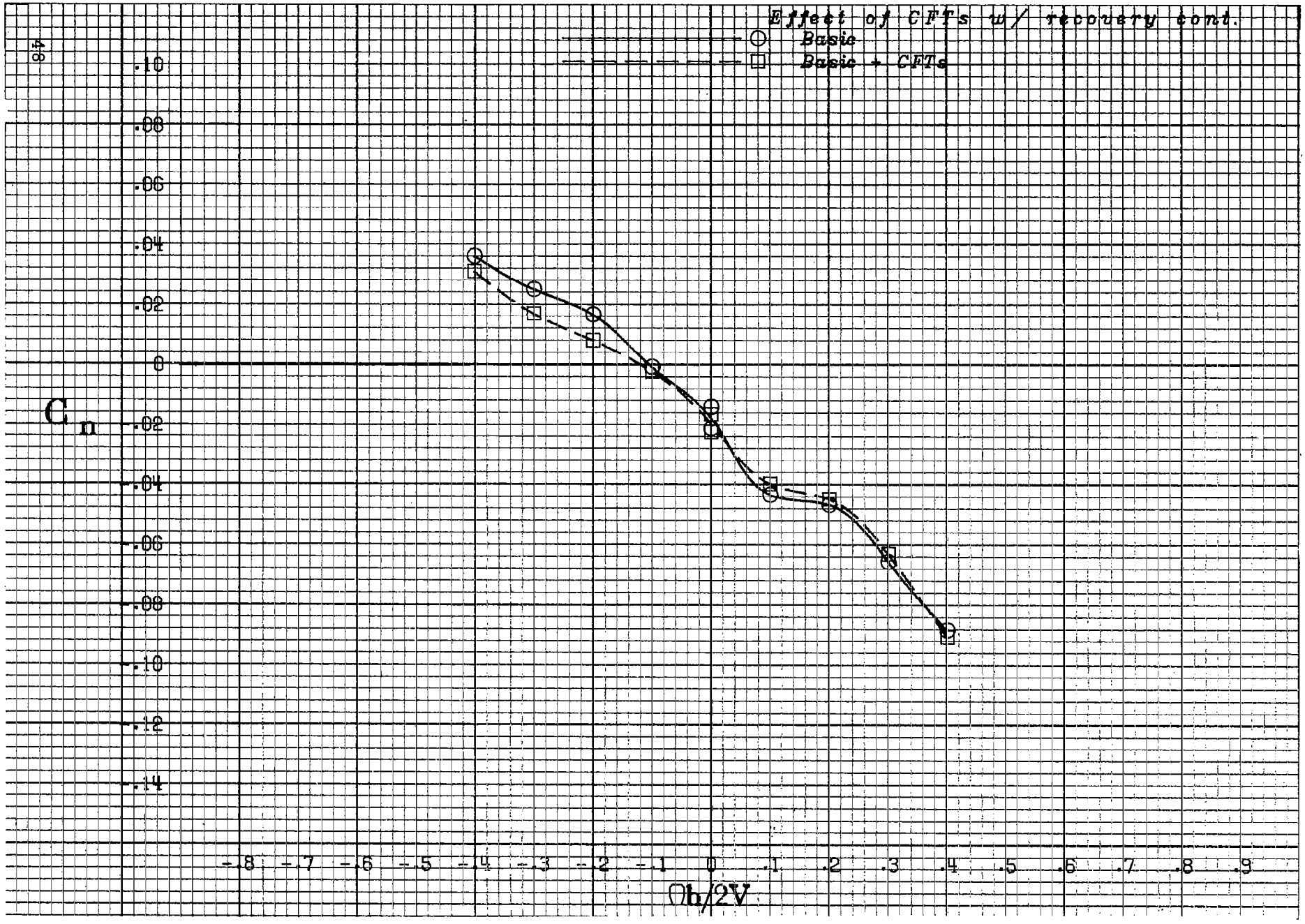

b) 70^{o} angle of attack.

Figure 12.- Continued.

c) 60^{o} angle of attack.

Figure 12.- Continued.

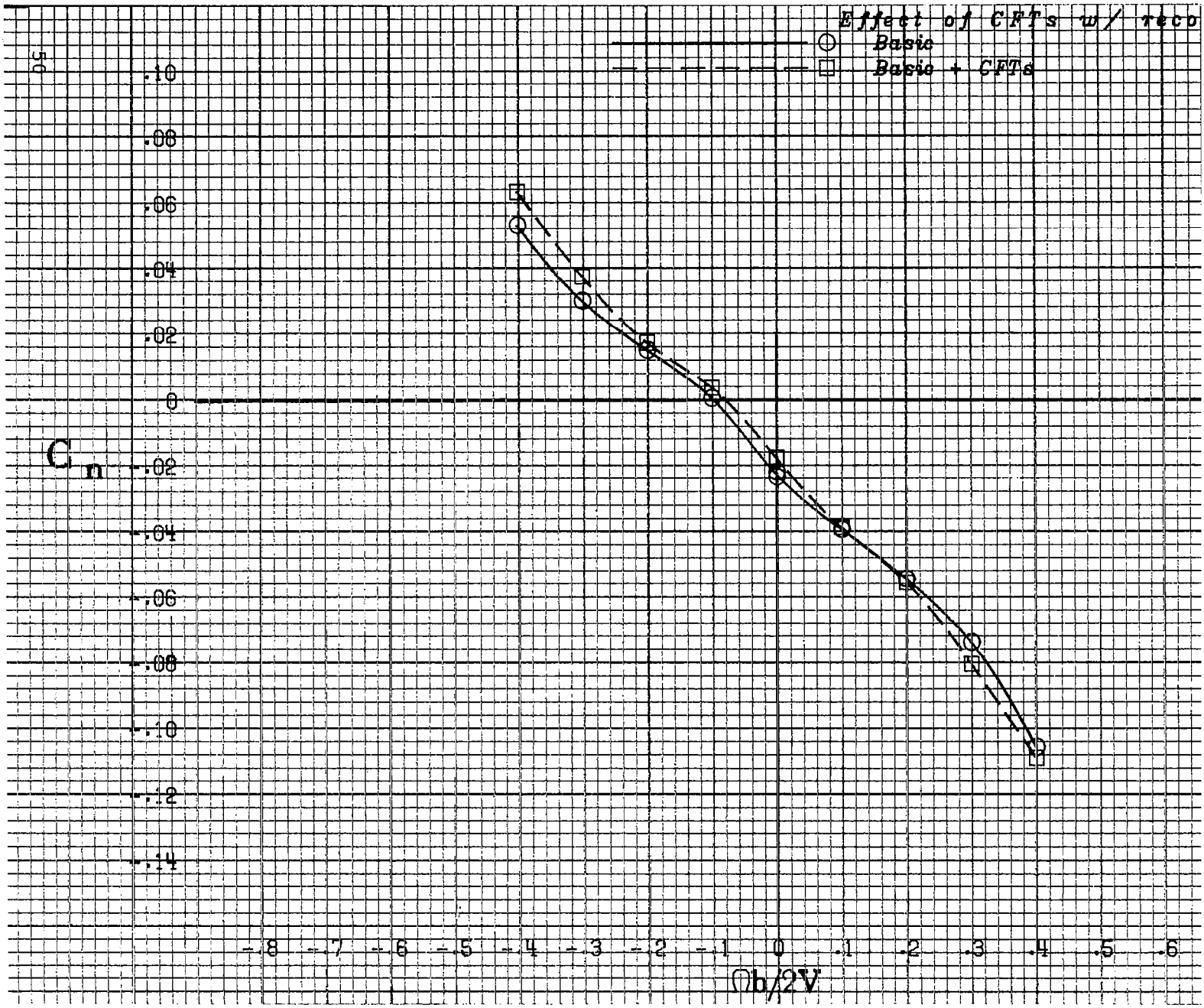

d) 40° angle of attack.

Figure 12.- Concluded.

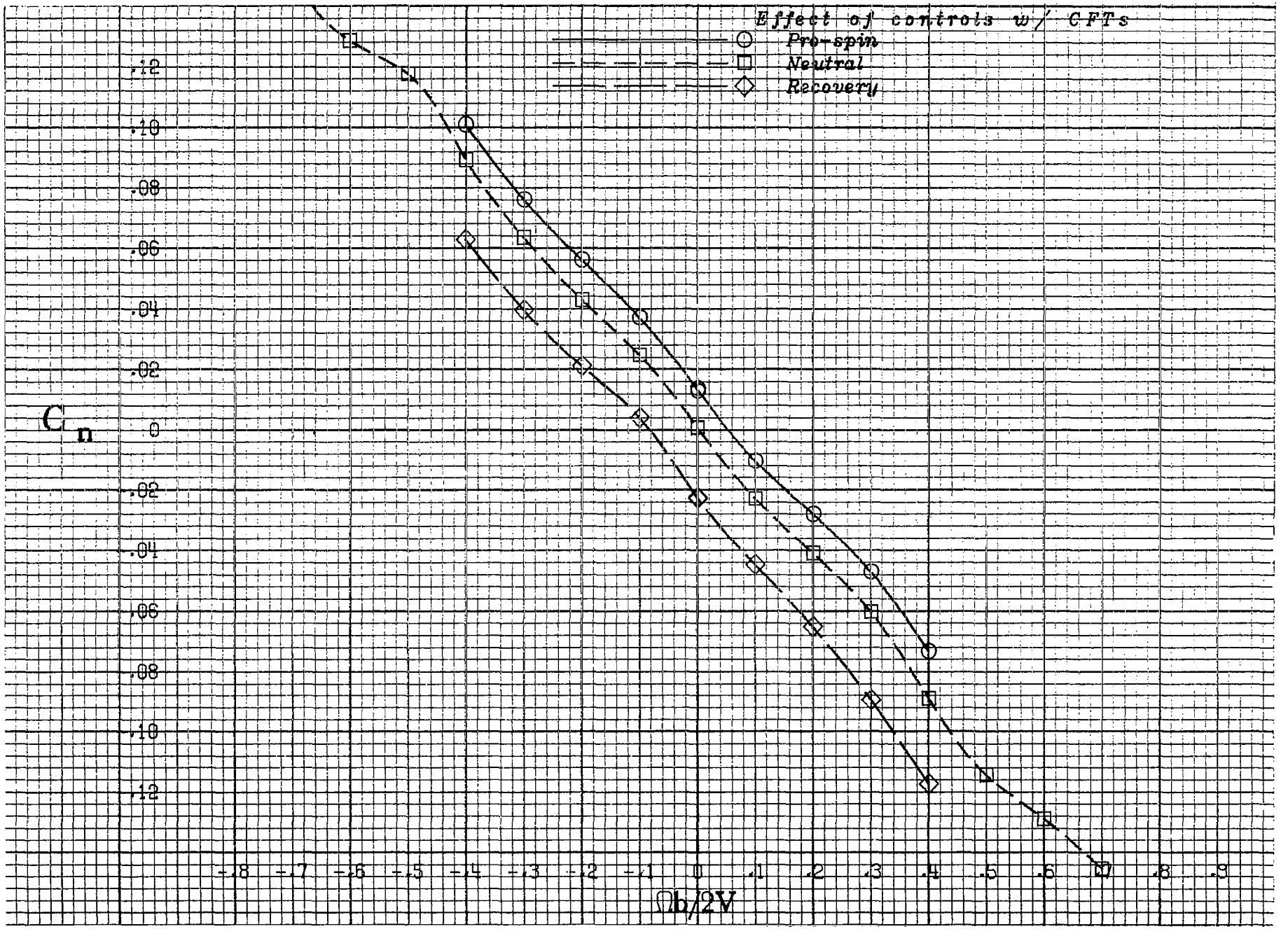

a) 30° angle of attack.

Figure 13.- Effect of control deflections on the yawing-moment coefficient for the basic airplane with conformal tanks.

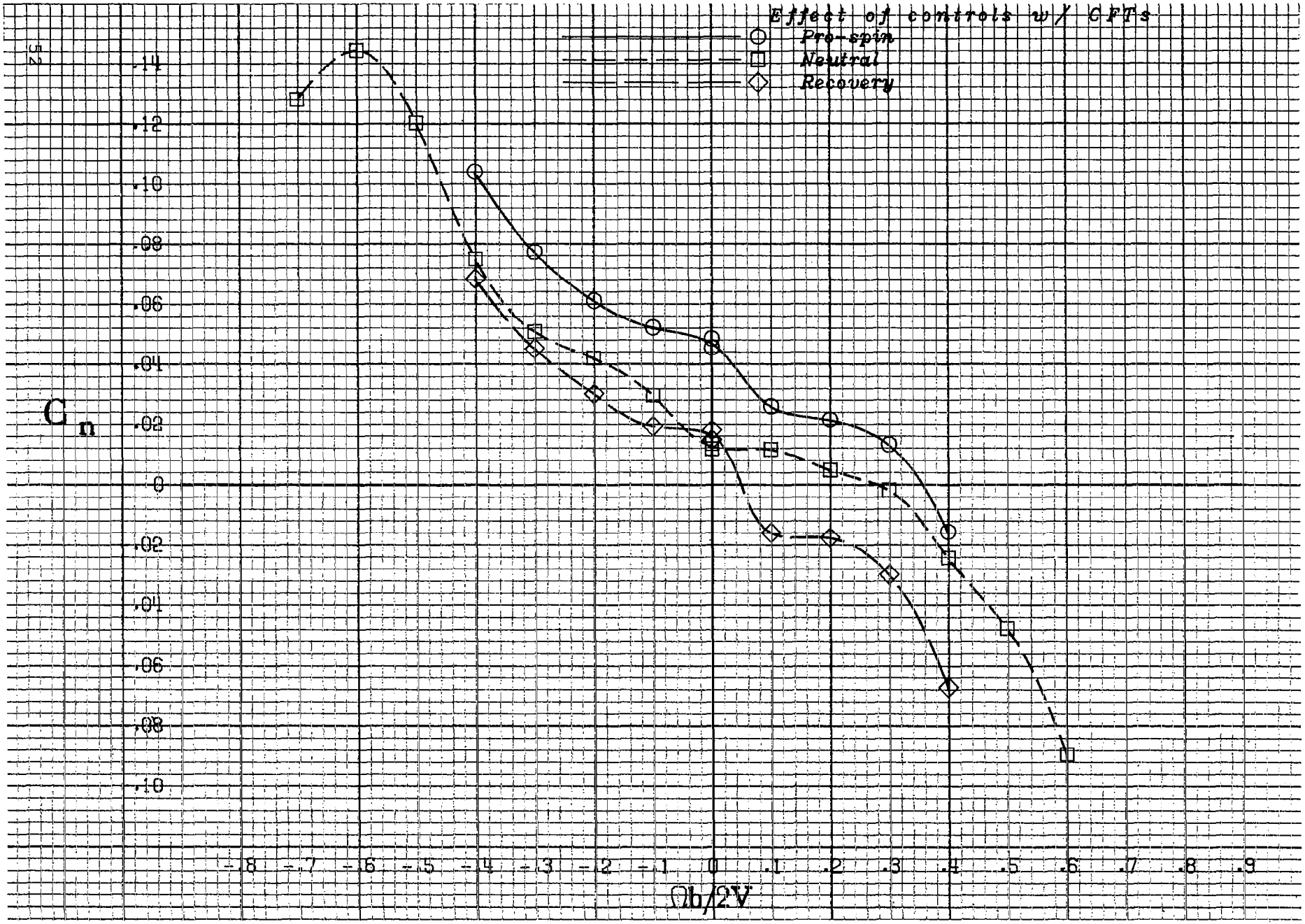

b) 50^{o} angle of attack.

Figure 13.- Continued.

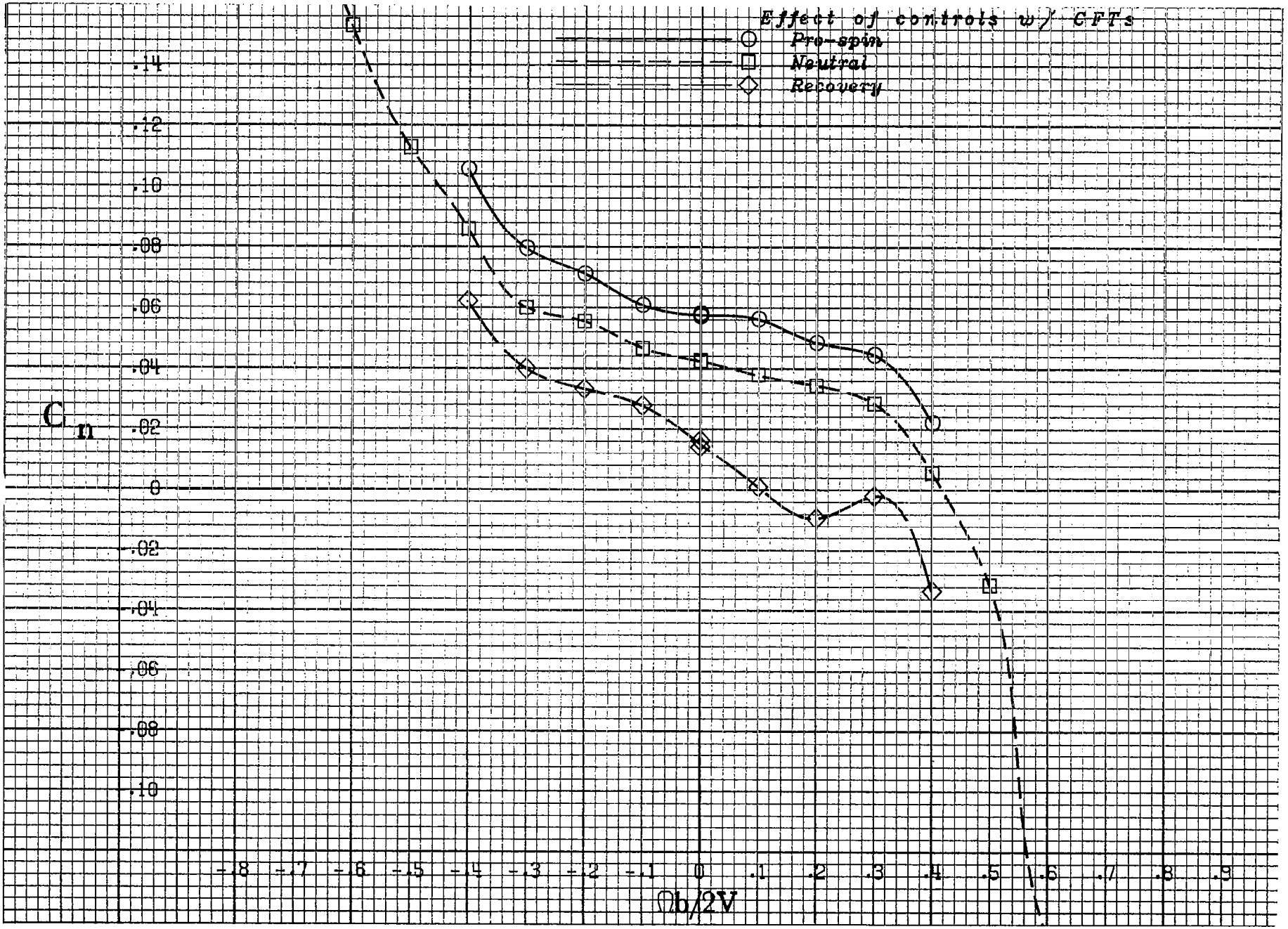

c) 60^{o} angle of attack.

Figure 13.- Continued.

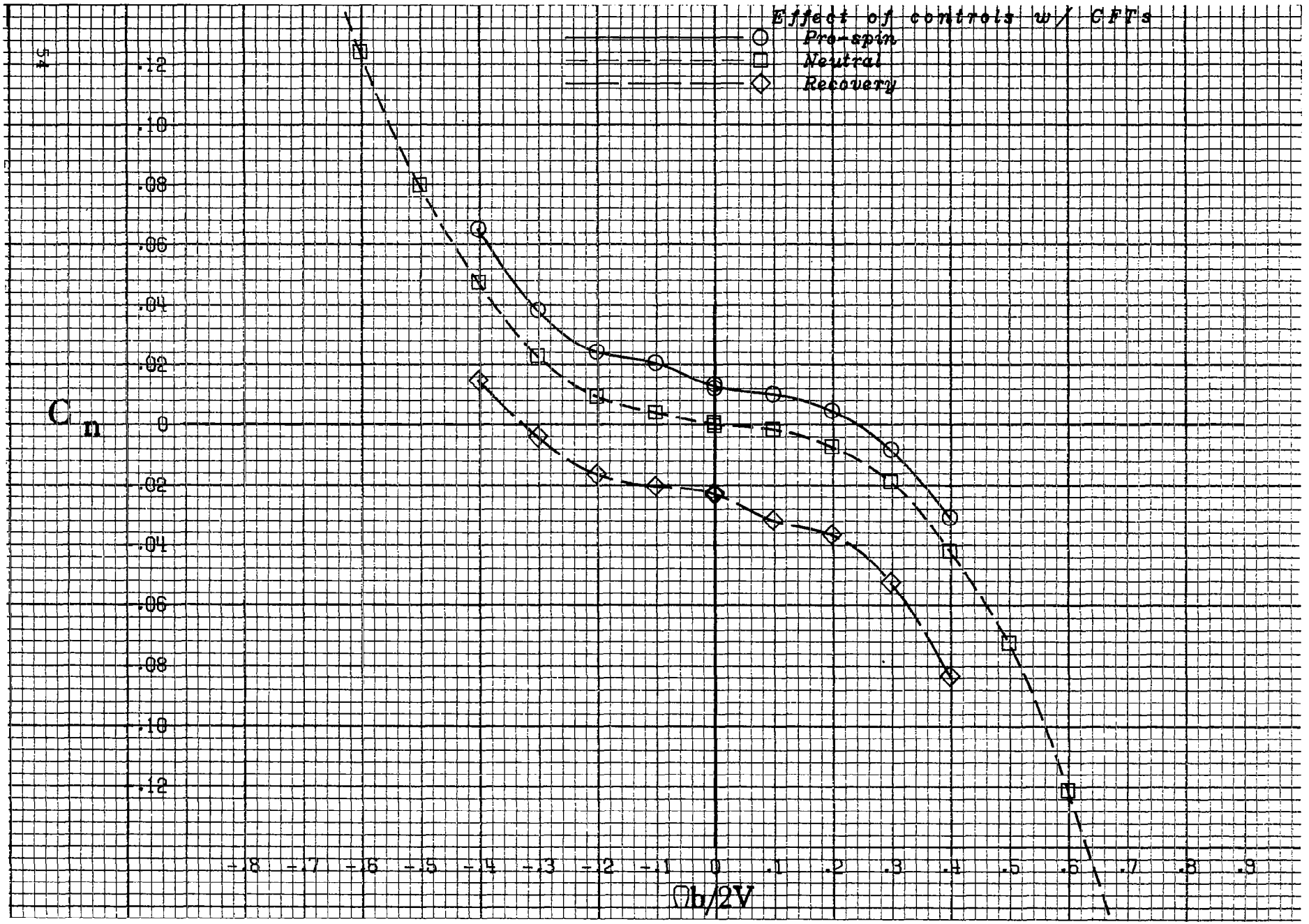

d) 80° angle of attack.

Figure 13.- Concluded.

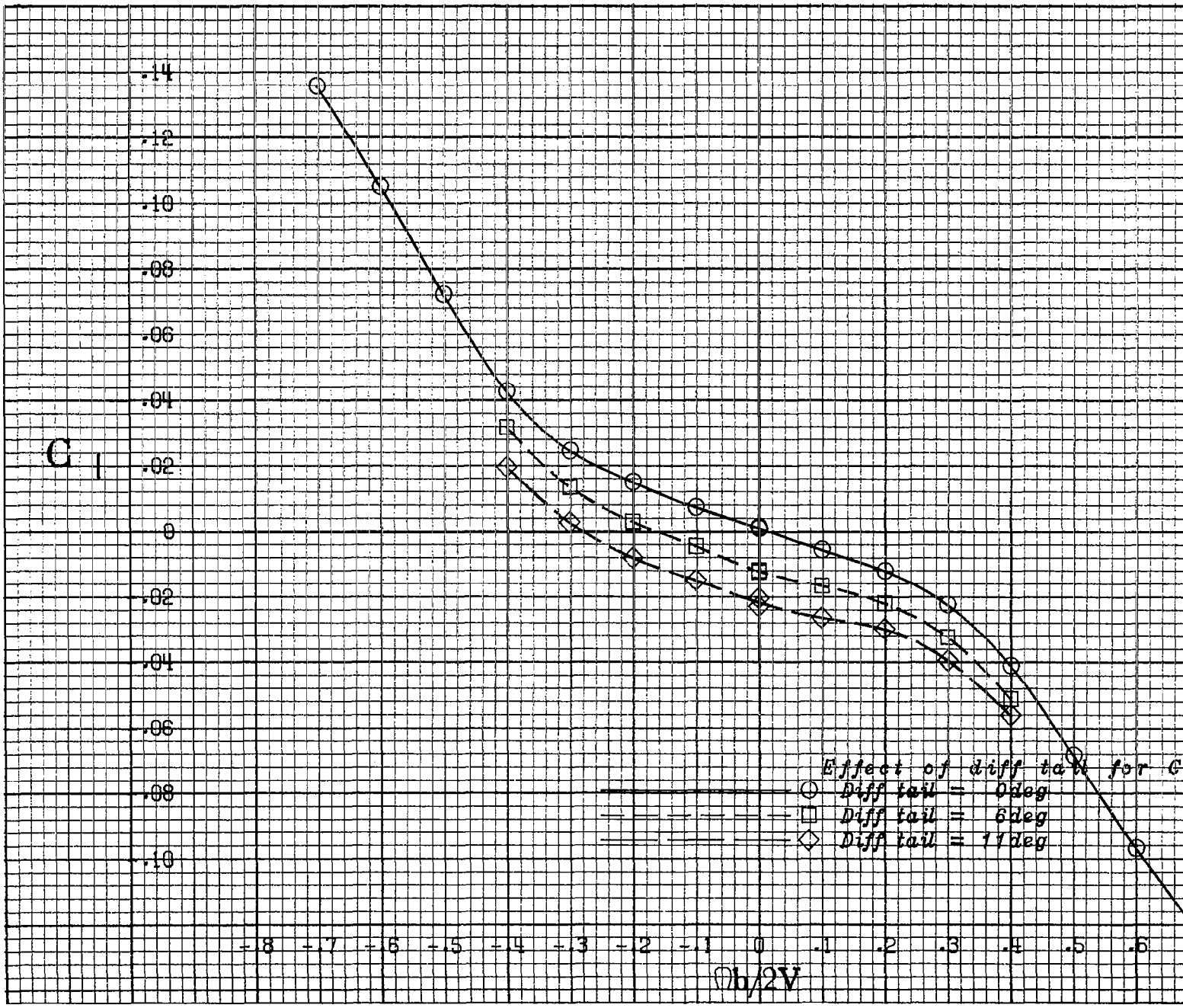

a) 20^{o} angle of attack.

Figure 14.- Effect of differential tail deflection on the rolling-moment coeffi
for the basic airplane with conformal tanks, all other controls neutral.

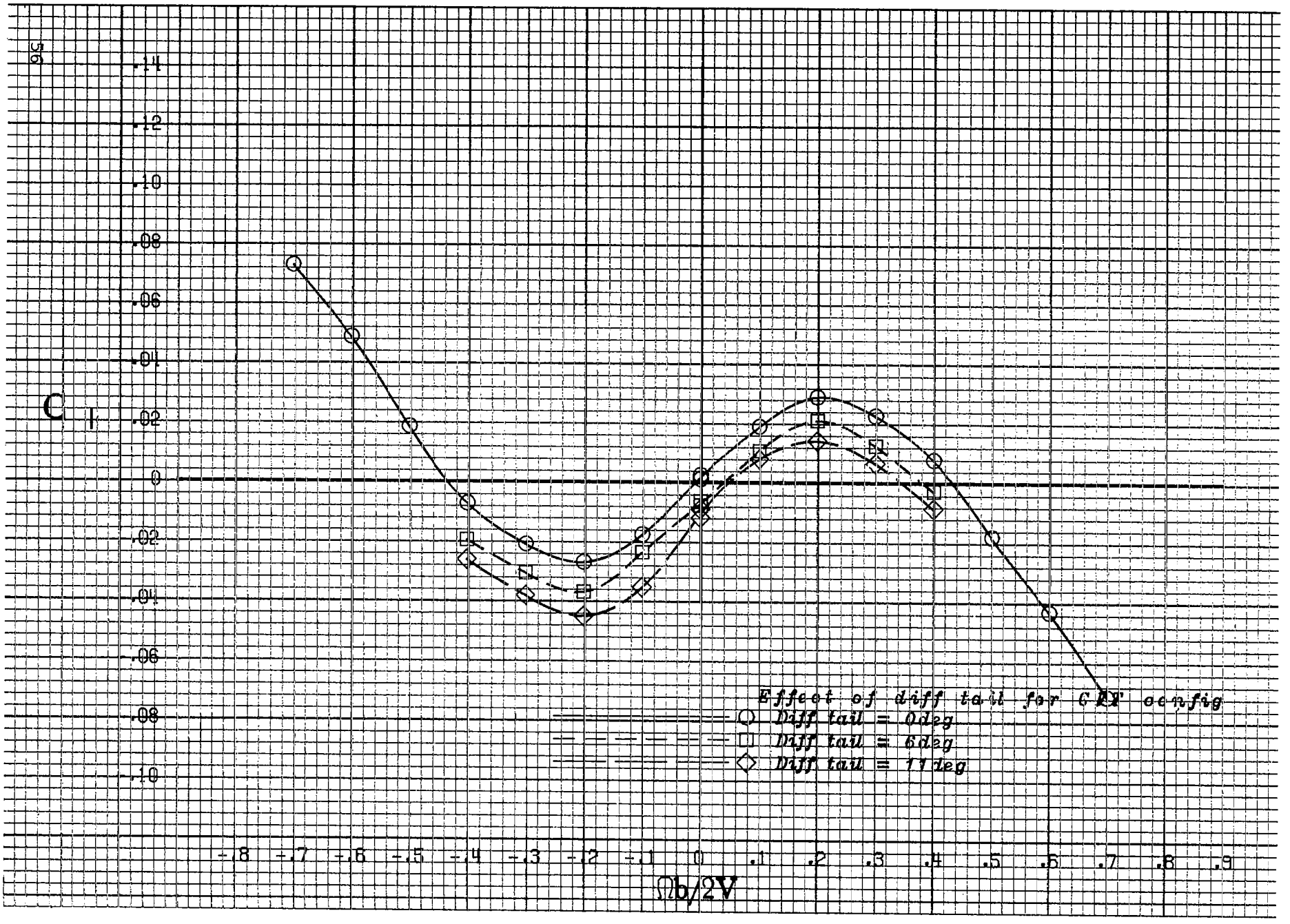

b) 30^{o} angle of attack.

Figure 14.- Continued.

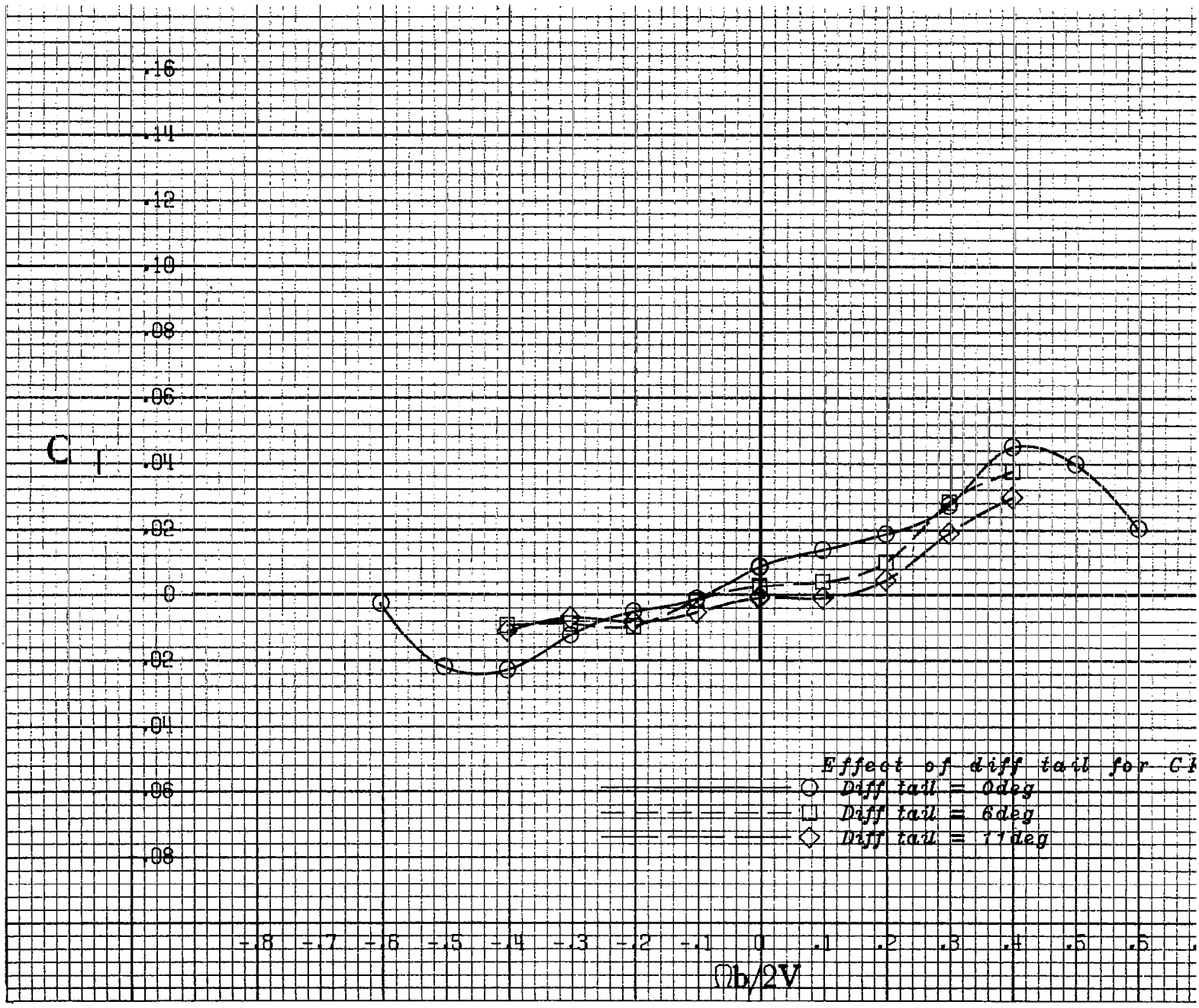

c) 40° angle of attack.

Figure 14.- Continued.

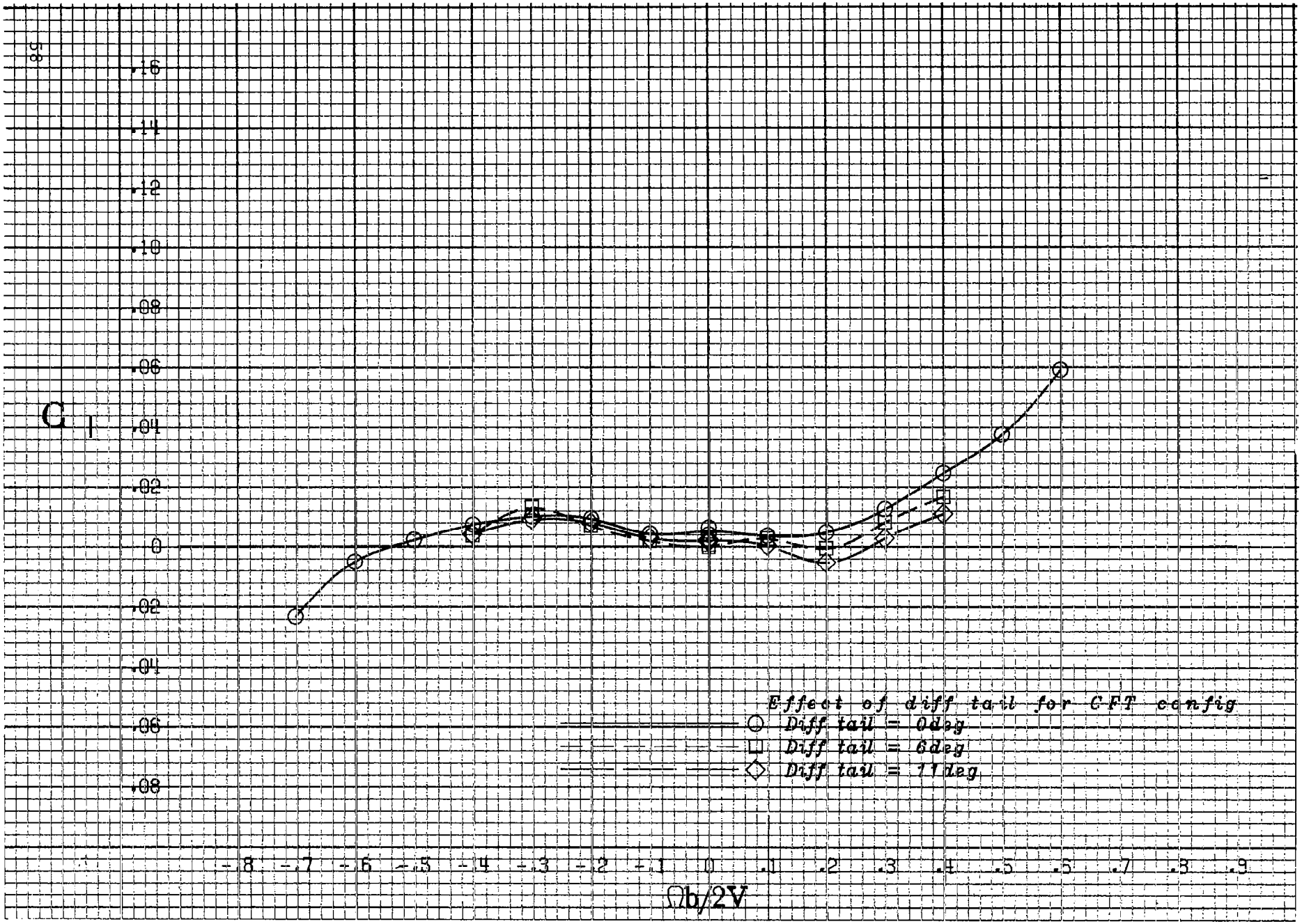

d) 50^{o} angle of attack.

Figure 14.- Continued.

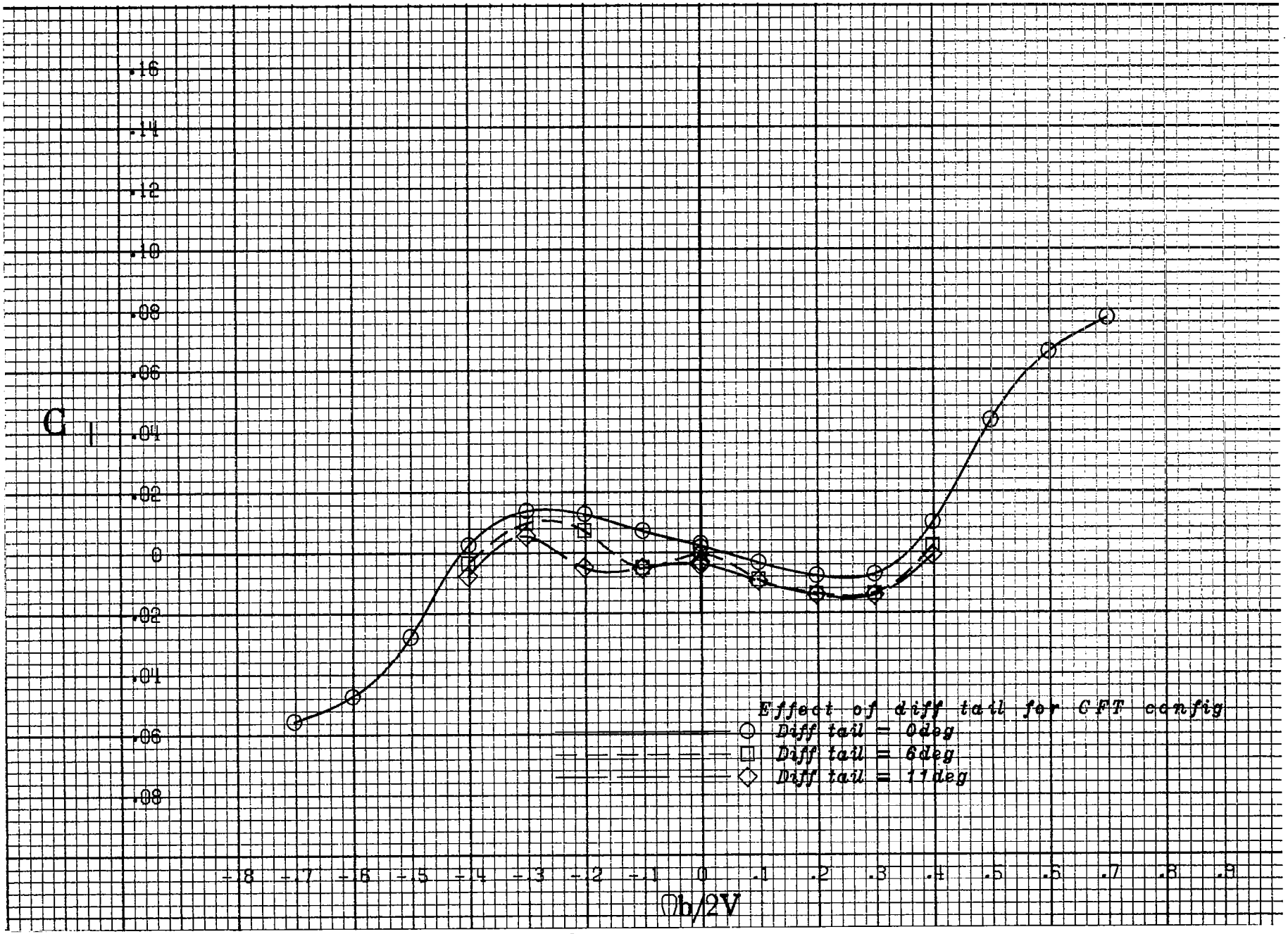

e) 70° angle of attack.

Figure 14.- Concluded.

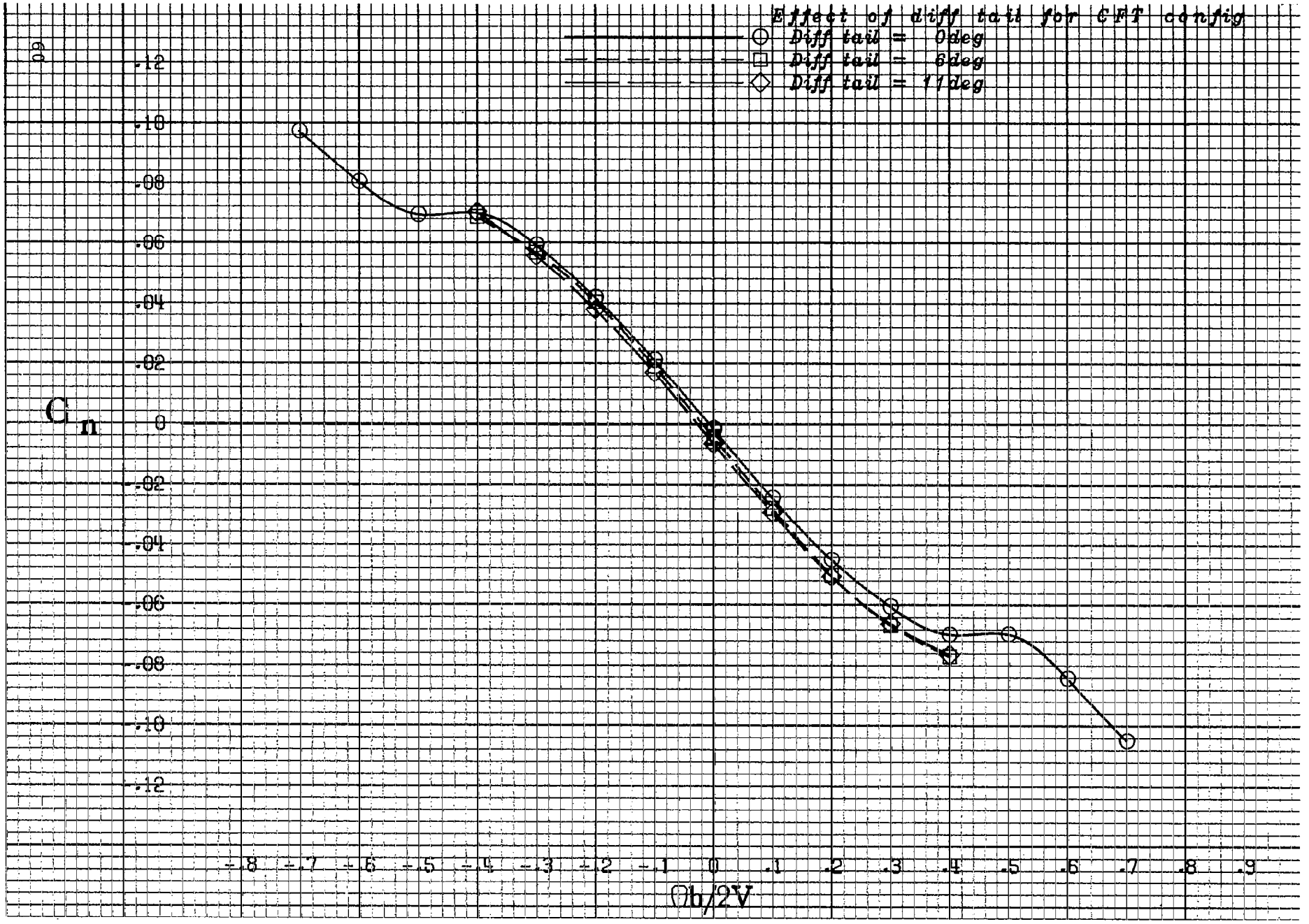

a) 20° angle of attack.

Figure 15.- Effect of differential tail deflection on the yawing-moment coefficient for the basic airplane with conformal fuel tanks, all other controls neutral.

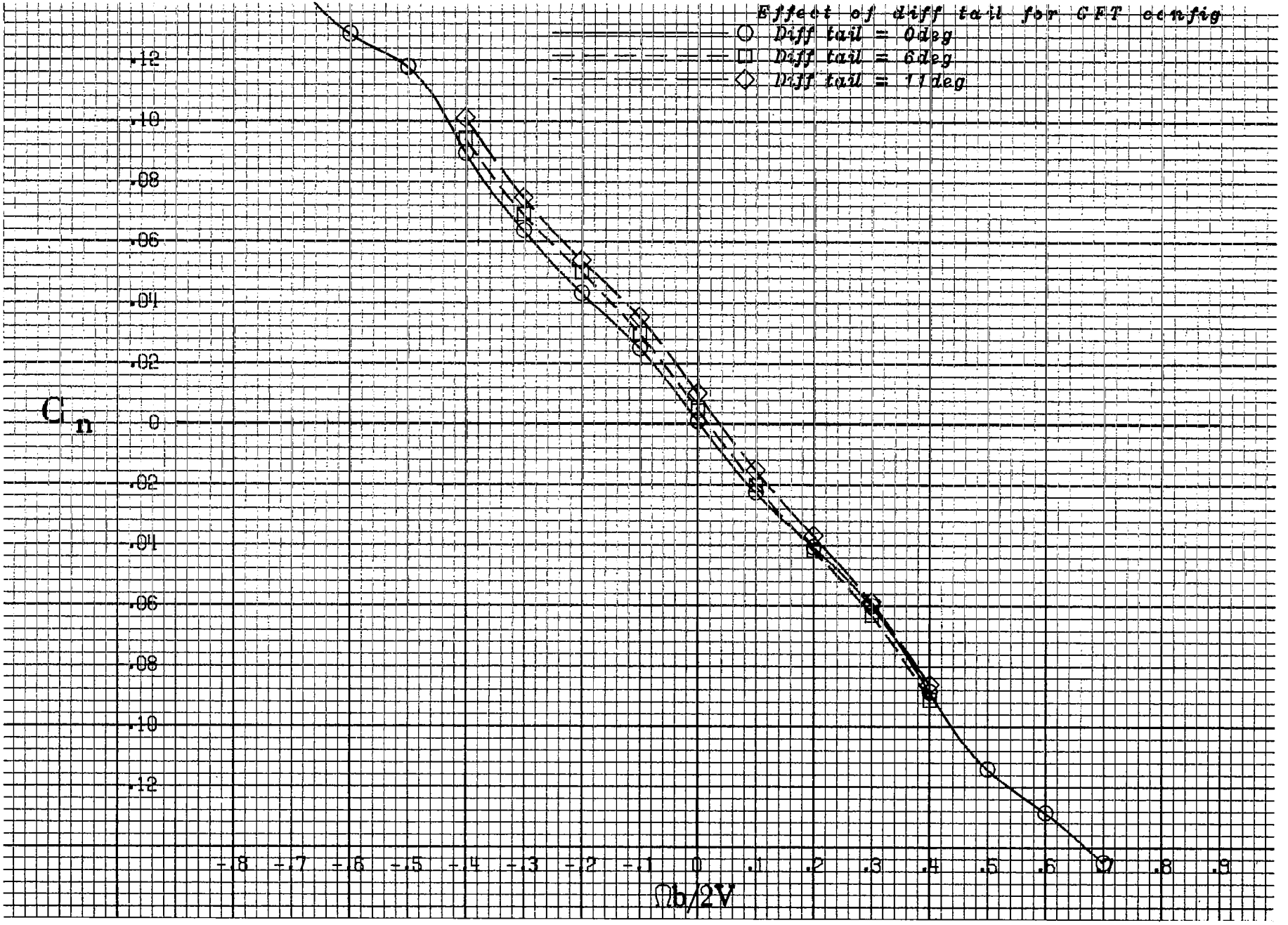

b) 30° angle of attack.

Figure 15.- Continued.

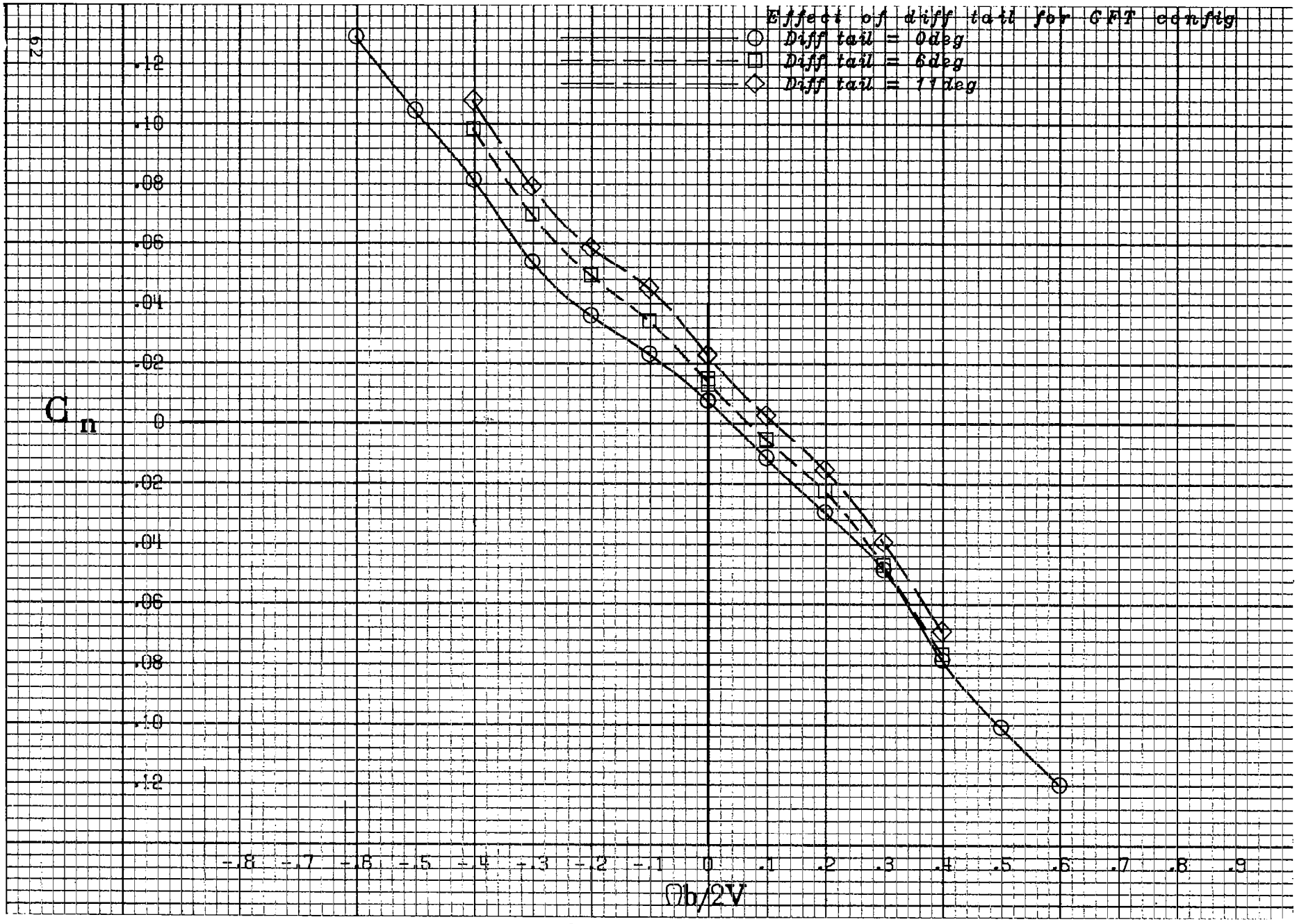

c) 40° angle of attack.

Figure 15.- Continued.

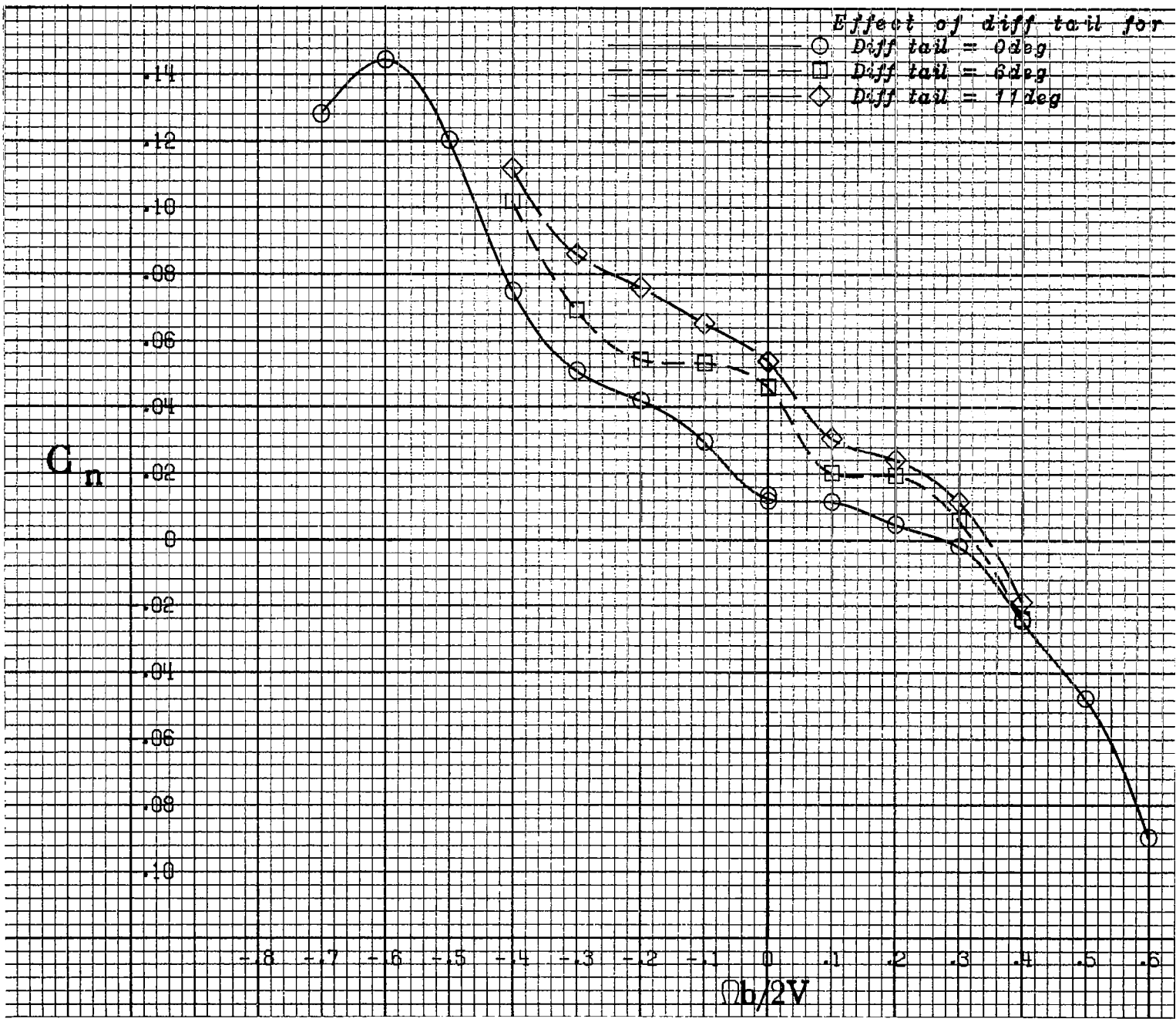

d) 50° angle of attack.

Figure 15.- Continued.

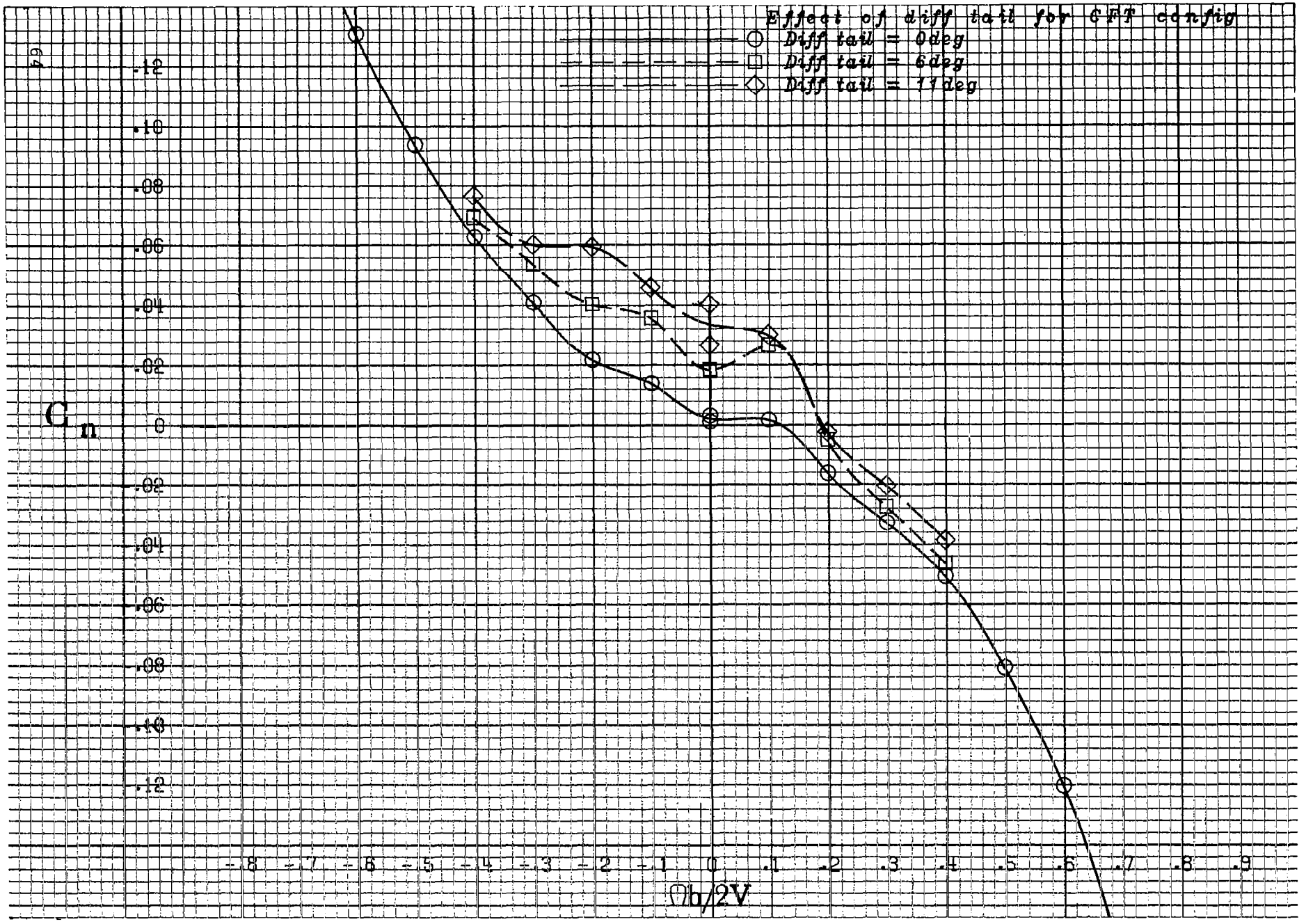

e) 70° angle of attack.

Figure 15.- Concluded.

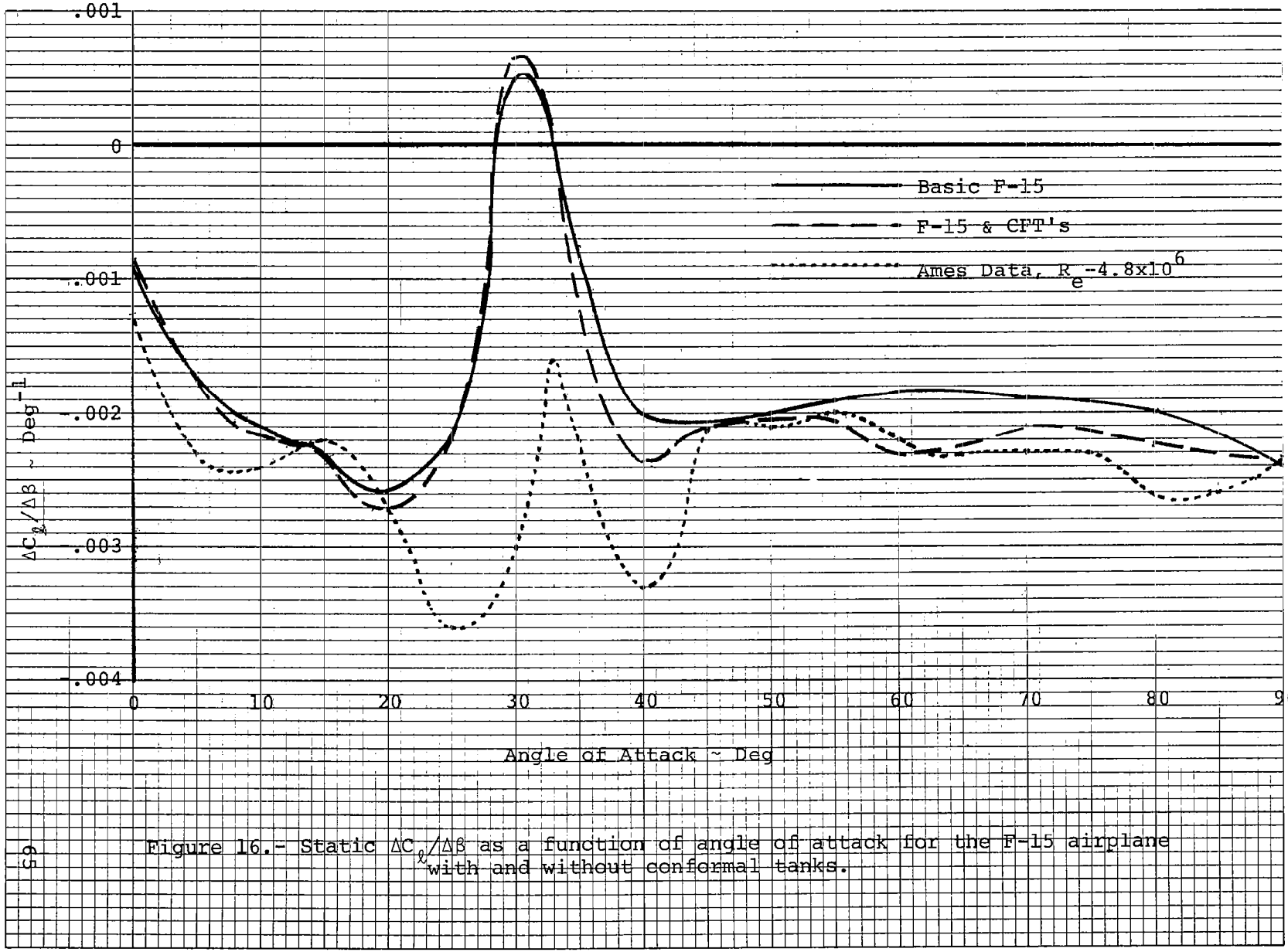

Figure 16.- Static $\Delta C_\ell/\Delta\beta$ as a function of angle of attack for the F-15 airplane with and without conformal tanks.

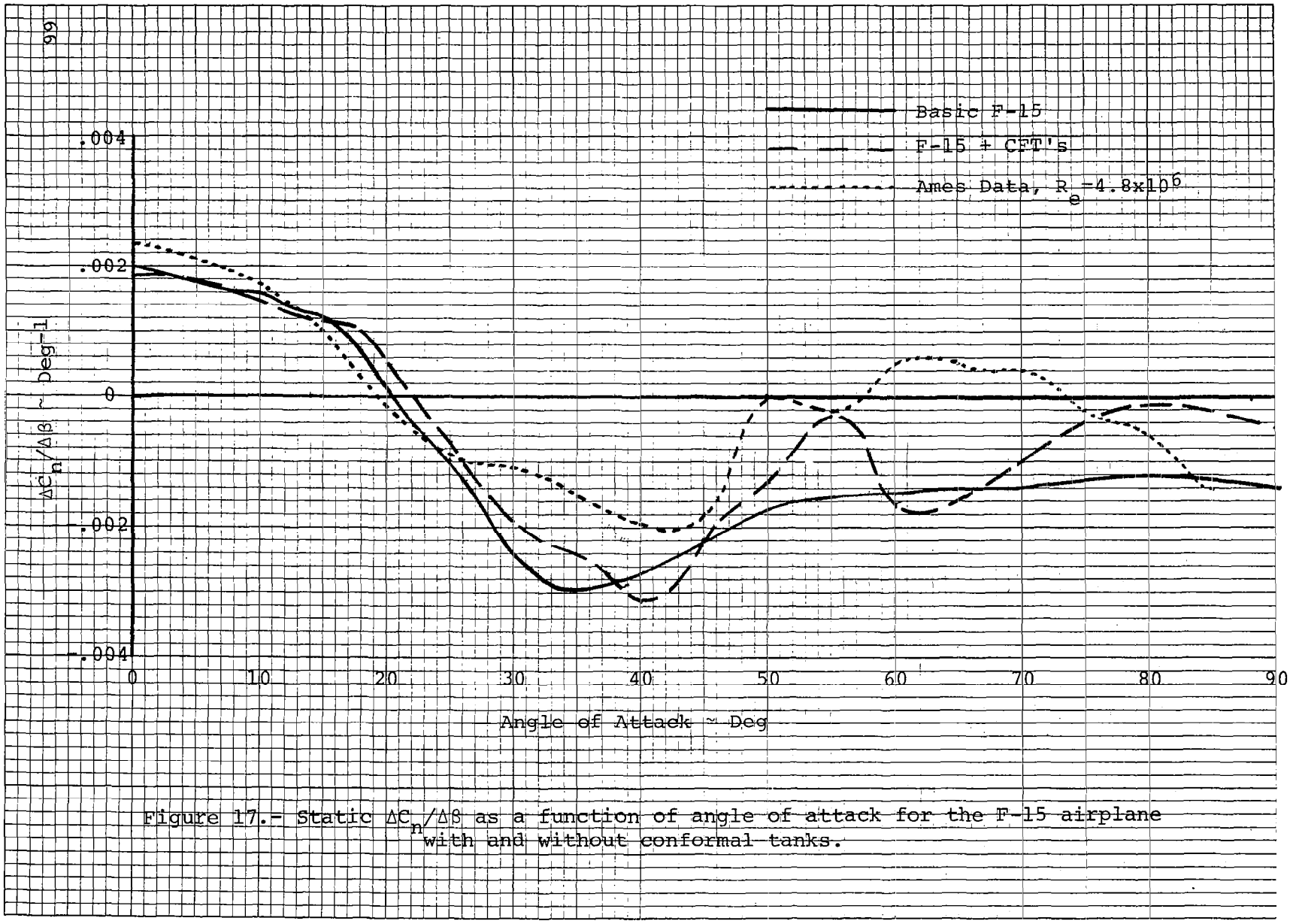

Figure 17.- Static $\Delta C_n/\Delta\beta$ as a function of angle of attack for the F-15 airplane with and without conformal tanks.

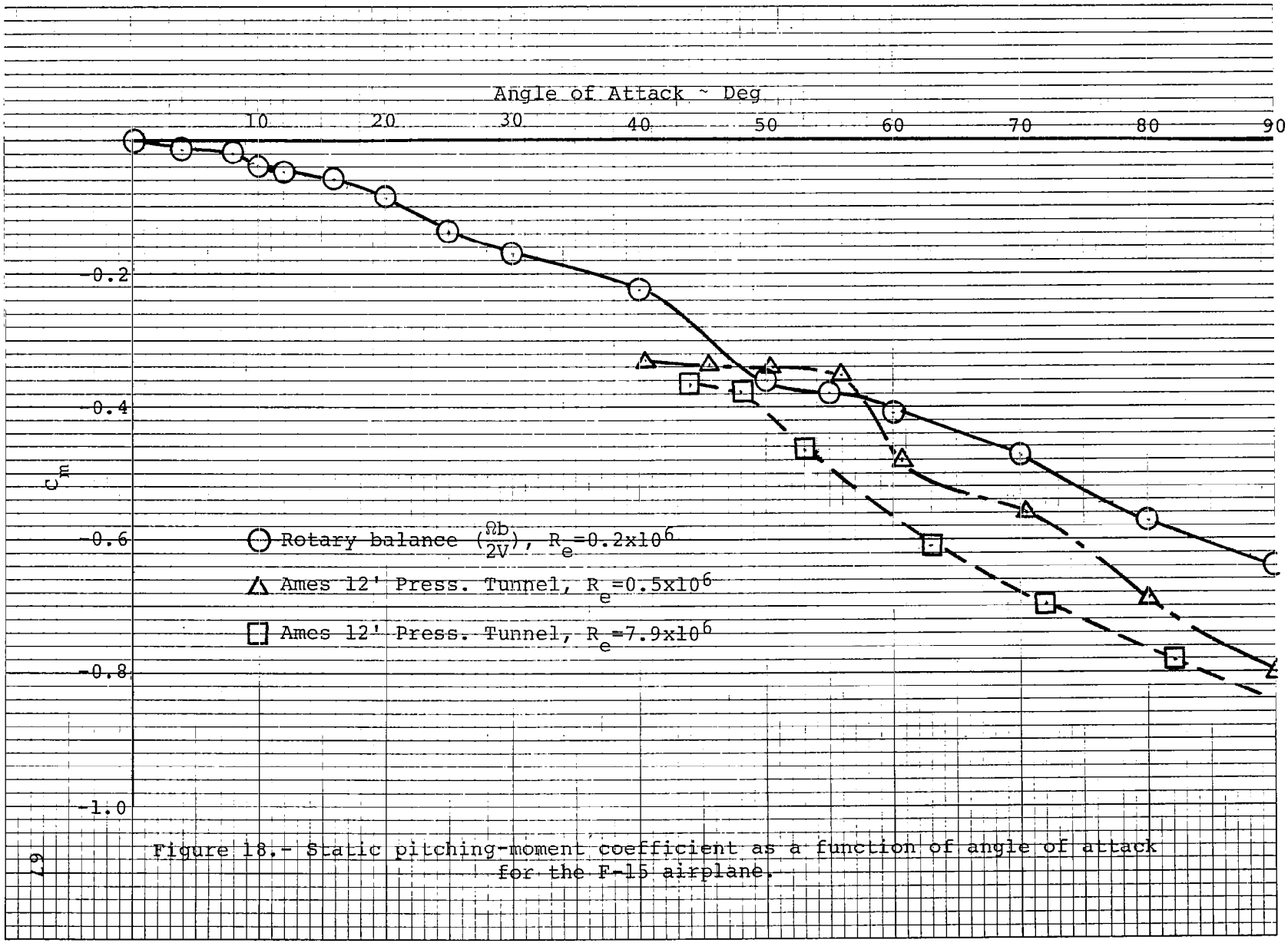

Figure 18.- Static pitching-moment coefficient as a function of angle of attack for the F-15 airplane.

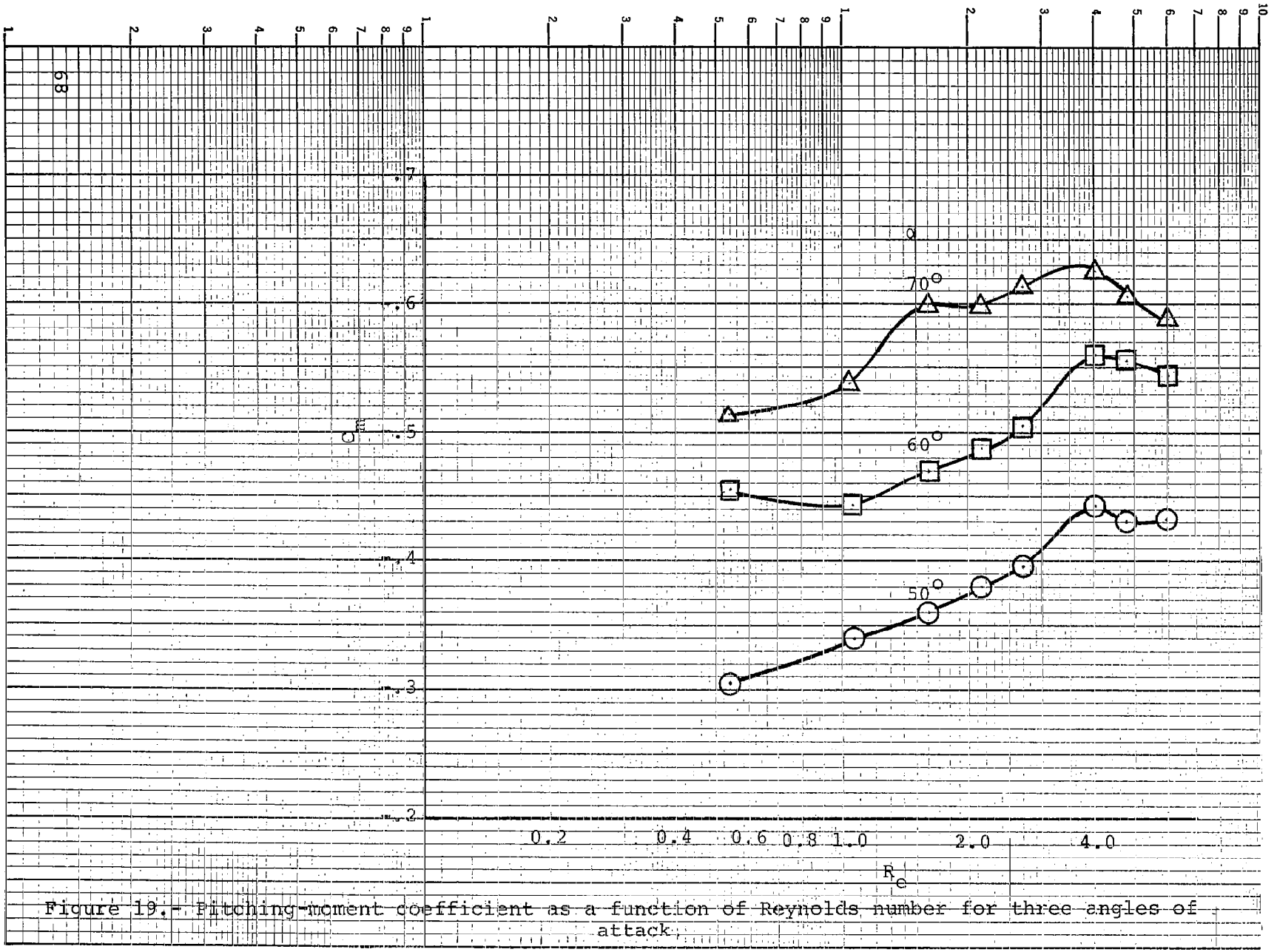

Figure 19.- Pitching-moment coefficient as a function of Reynolds number for three angles of attack.

1. Report No.	2. Government Accession No.	3. Recipient's Catalog No.
NASA CR-3479		

4. Title and Subtitle	5. Report Date
ANALYSIS OF ROTARY BALANCE DATA FOR THE F-15 AIRPLANE INCLUDING THE EFFECT OF CONFORMAL FUEL TANKS	April 1982
	6. Performing Organization Code
7. Author(s)	8. Performing Organization Report No.
Billy Barnhart	
	10. Work Unit No.
9. Performing Organization Name and Address	11. Contract or Grant No.
Bihrle Applied Research, Inc. 400 Jericho Turnpike Jericho, New York 11753	NAS1-16205
	13. Type of Report and Period Covered
12. Sponsoring Agency Name and Address	Contractor Report
National Aeronautics and Space Administration Washington, DC 20546	14. Sponsoring Agency Code 505-43-13-01

15. Supplementary Notes

Langley Technical Monitor: James S. Bowman, Jr.

Topical report

16. Abstract

F-15 rotary balance data have been analyzed, and the influence of control deflections, Reynolds number and airplane components, i.e., body, wing, horizontal and vertical tails, as well as conformal tanks, on the aerodynamics up to 90 degrees angle of attack are discussed. Steady-state spin mode predictions using these data are presented, which show excellent correlation with spin tunnel and flight test results.

Generally, the data shows damped yawing moment slopes with rotation at all angles of attack, and good control effectiveness. Differences in the rotary aerodynamics due to the addition of conformal tanks are minimal. The small differences in the region of the flat spin do, however, indicate that the resulting spin mode would be slightly flatter and faster for a conformal tank equipped airplane. The addition of conformal tanks also may make the airplane more departure susceptible.

17. Key Words (Suggested by Author(s))	18. Distribution Statement
Spinning Rotary balance High angle-of-attack wind tunnel data	Unclassified-Unlimited Subject Category 02

19. Security Classif. (of this report)	20. Security Classif. (of this page)	21. No. of Pages	22. Price*
Unclassified	Unclassified	70	A04

For sale by the National Technical Information Service, Springfield, Virginia 22161

NASA-Langley, 1982